Cure Monitoring of the Liquid Composite Molding Process Using Fiber Optic Sensors

by

Dara L. Woerdeman
Materials Science & Engineering Department
The Johns Hopkins University
Baltimore, MD 21218

Julie K. Spoerre
Department of Technology
Southern Illinois University at Carbondale
Carbondale, IL 62901

Kathleen M. Flynn and Richard S. Parnas
Polymers Division
National Institute of Standards & Technology
Gaithersburg, MD 20899

ABSTRACT

Fluorescence has been demonstrated to be an accurate tool for monitoring resin cure and is measured using an evanescent wave fiber-optic sensor. An economical optical fiber sensor has been developed with a refractive index over 1.6, permitting evanescent wave monitoring of epoxy resins. The fluorescence wavelength-shift, which has been correlated with monomer conversion, is monitored during the liquid molding process.

Unidirectional glass fabrics, at volume fractions from 40-60%, were injected with epoxy resin at a variety of driving pressures and cured at several temperatures. Several composite parts were fabricated to test the effects of vacuum pressure, injection rate, cure temperature, and fiber volume fraction on the performance of the sensor.

The sensitivity of the evanescent wave fluorescence sensor to the condition of the resin system was also examined. Two sets of resin/hardener samples were subjected to rigorous chemical analysis to determine the extent of their differences.

INTRODUCTION

Liquid Composite Molding (LCM) is a versatile and economically attractive technique for fabricating polymer composites of various sizes, shapes, and performance characteristics (1). In the basic process, a fiber preform is inserted into a mold. The heated mold is then closed and filled with a reactive prepolymer and time is allowed for polymerization. When the composite part has gained sufficient strength, it is demolded. The principal advantage of LCM over other composite forming processes is its ability to make large parts of complex shape at a lower cost.

LCM has only recently been employed in mass production environments requiring fast cycle times. Process conditions are typically determined empirically with molding experiments, making process development prohibitive and processing parameters difficult to optimize. In-situ monitoring for on-line quality control of polymer composite processing is widely recognized as an effective means of driving down part cost by minimizing part to part variation. In the present work, a fiber optic cure sensor was developed and incorporated into a high volume fraction preform during LCM. Because the extent of cure is an important process variable, a number of in-mold cure sensors have previously been developed based on ultrasonic, dielectric, optical, and spectroscopic methods (2). Advantages and disadvantages are associated with each technique, a few of which are discussed below.

Cure Sensors

The attenuation and phase velocity of ultrasonic waves in epoxy resins have been found to vary during the cure process (2,3). Attenuation data obtained with the shear wave reflection technique (3) have been reliably correlated with the extent of reaction (2). Additionally, an ultrasonics wave propagation method has been developed to measure rheological properties of the curing resin. The rheological properties of curing resins govern the extent to which consolidation of reinforcement plies and build up of residual stresses occur during processing (3). However, one of the main drawbacks of this technique is the current cost of the probe, which is too expensive to be discarded after a test and must be reused. Other disadvantages include limitations on the range of temperatures and environmental conditions that can be investigated (3).

Dielectric measurements have been shown to have many advantages for cure monitoring because the electrical parameters are sensitive to molecular mobility (2,4). Studies of thermosets have shown well defined changes in conductance during the course of the curing reaction (3,4).

Mijović et al. (5) demonstrated that changes in impedance during cure of reactive polymers can be related to the degree of cure obtained by other techniques, such as infrared spectroscopy. In addition, they developed empirical correlations between impedance and chemorheological changes, namely, gelation and vitrification (5).

An important technical barrier which has impeded wider usage of dielectric spectroscopy is the intrusive nature of commercially available dielectric sensors to the finished composite part (2). It has also been indicated that the usefulness of dielectric loss measurements during the initial stages of cure is complicated by the conductivity of adventitious ions present in the system (3,6). However, other researchers argue that ionic impurities represent but one contribution to the measured apparent or overall conductivity (5).

Previously developed ultrasonic and dielectric sensors also suffer other drawbacks. They cause resin rich areas and measure the degree of cure averaged over a large volume of the mold (2). However, the resin cure kinetics can vary substantially across the thickness of the mold due to thermal effects. The cure kinetics close to the fiber surface may also vary substantially from the bulk resin cure kinetics due to surface induced chemical potential gradients (7). In rating the various on-line monitoring techniques, Hunston et al. (2) emphasized the importance of the size of the embedded sensor since this governs the degree to which the sensor can perturb the part performance. For this reason, spectroscopic and optical methods were rated as the most versatile since the embedded sensors are based on fiber optics.

Fiber Optic Cure Sensors

An optical method for monitoring the cure of epoxies has been reported by Afromowitz and depends upon the increase in the index of refraction during cure (8). Conventional step index or graded index fibers were used to guide light to and from a sensor element, fabricated from epoxy. The epoxy sensor, which had been cured in advance, was placed in contact with the uncured epoxy sample. The number of guided modes that the sensor could support decreased progressively as the state of cure of the surrounding resin increased, causing a decrease in the transmitted intensity as a function of time (8).

Fiber optic Raman spectroscopy has been used for cure monitoring of a neat epoxy/amine system using a fused-silica distal mode optical fiber sensor, which monitors a volume of material in the shape of a cone at the fiber terminus (9,10). This technique was applied to liquid molding of a high volume fraction composite however, in a form that required the user to insert the distal end of the fiber into a Teflon tube that had been

previously filled with the epoxy mixture (11). In this configuration the probe was incapable of monitoring the resin actually used to fabricate the composite part. Furthermore, the authors suggested that the determination of percent cure in the industrial sample was not as precise as the laboratory sample mainly due to the fluorescence from surrounding glass fibers and nylon bindings which contributed to a higher background (11).

Fluorescence monitoring has been used with distal mode optical fiber sensors for monitoring the flow during injection molding, as well as for cure monitoring (12-16). Levy and Schwab (12) developed a fluorescence-based fiber-optic distal end sensor and monitored changes in the intrinsic fluorescence intensity of a graphite-epoxy laminate during cure in an autoclave. During autoclaving, the intensity of the signal peaked and then began to decline instead of continuing to increase at a rate that corresponds to the slower rate of cure (12). They attributed this result to an instrumental effect and explained that the next step would be to develop an empirical correction to the signal intensity. Levy and Schwab also observed shifts in the wavelength of the fluorescence emission maximum and correlated this signal with degree of cure for the late stages of isothermal cure. Wang and Fanconi (6) rejected intrinsic fluorescence monitoring in their work, because they observed batch-to-batch variations in their spectral response and because the approach could not be generalized to other epoxy systems. Instead, they used fluorescent probes that respond to the local environment by changes in intensity.

Dang and Sung (16) designed a distal-end fiber optic fluorometer for in-situ monitoring of a diamine cured epoxy. Epoxy samples used for cure studies were stoichiometric mixtures of diglycidyl ether of bisphenol A (DGEBA) and diaminodiphenyl sulfone (DDS), into which 0.01% by weight of the fluorophore, 4,4'-diaminoazobenzene (DAA), was dissolved. One of the objectives of their study was to find a suitable internal reference dye for use in conjunction with DAA. Sulfo-rhodamine 101 (SRH) was found to be satisfactory because it is non-reactive, thermally stable, highly fluorescent, viscosity-insensitive, and its emission range is far removed from that of DAA (16). All of the above distal-mode optical fiber sensors take measurements in a compact sensing volume of approximately 10^{-3} cm^3, and a separate sensor is required to obtain measurements from each desired location in the mold.

A different fiber optic sensing geometry, evanescent wave sensing, offers the possibility of distributed sensing with a single fiber and of a surface sensitive measurement indicative of the development of the critical resin/fiber interface. Evanescent wave sensing has been applied to resin cure monitoring of graphite fiber/polyimide composites by

employing mid-infrared transmitting optical fiber sensors (17). While there are advantages to using mid-infrared spectroscopy, it often requires using fibers that are large, fragile, costly, potentially toxic, have poor transmission, and undergo physical aging.

Evanescent wave sensing has also been applied to resin cure monitoring of neat epoxide/amine samples by utilizing UV/visible transmitting fibers to monitor fluorescence emission (18,19). Fuchs and Sung (19) have developed and used a sapphire optical fiber coupled to a silica transmission fiber for evanescent wave sensing of epoxy/amine reactions. Sapphire optical fibers are notorious for their poor transmission properties and high cost. The authors measured the fluorescence intensity of a 1% DAA solution in DGEBA and tracked the increase in DAA peak intensity during cure. Fuchs and Sung also compared the normalized intensities obtained by the evanescent sensor with those from the distal end fiber optic sensor and suggested that the evanescent wave data exhibited faster reaction rates than the distal end data.

In an evanescent wave fluorescence sensor, fluorescent probes in the resin surrounding the sensor fiber are excited by the electric field in the wave situated at the fiber/resin interface, as illustrated in Figure 1 (6,18-20). Evanescent wave sensors require the refractive index of the sensor to be larger than the refractive index of the surrounding medium, as the evanescent wave arises from total internal reflection at the waveguide/medium interface. The evanescent wave extends beyond the reflecting interface into the surrounding medium and decays approximately exponentially in amplitude. The distance at which the electric field amplitude decreases to e^{-1} its original value is termed the depth of penetration (6,20). The penetration depth, d_p, is given by

$$d_p = \frac{\lambda}{2\pi n_1 \left(\sin^2\theta - (\hat{n}_2/n_1)^2\right)^{\frac{1}{2}}} \qquad (1)$$

where λ is the wavelength of light, n_1 is the refractive index of the fiber, $\hat{n}_2$ is the complex refractive index of the medium, and θ is the angle of incidence of the propagating light at the interface. The complex refractive index is given by $\hat{n}_2 = n_2 - ik_2$, where k_2, the extinction coefficient, is negligible for the fluorescence frequencies (6). Values for d_p are typically of order 10^2 nm to 10^4 nm. Fluorescent dye molecules that are located within an approximate distance d_p from the fiber/medium interface can be excited by the evanescent wave. Some of the fluorescence emitted by the probe molecules will be coupled back into the optical fiber and transmitted to the detector (21).

A fiber-optic evanescent fluorosensor, which allows a fraction of the fluorescence to tunnel back into the fiber upon evanescent excitation, was first proposed by Block and Hirschfeld (22) and later employed by Andrade et al. (23). Block and Hirschfeld (22) showed that one of the main advantages to using a fiber or rod over a planar waveguide or prism is that the fluorescence tunneling into bound modes of the fiber is efficiently transmitted to the fiber face for detection. According to Glass et al. (24), this results in higher brightness of the observed fluorescence and in the observed signal intensity being directly proportional to the length of fiber used.

Fluorophores

Fluorescent dyes have commonly been used to probe their molecular environments. For example, molecular rotor dyes have been used to monitor the cure of a thermoset material (6), as well as thermoplastic polymerization (14,25). Loutfy (25) examined the effects of physical changes occurring during radical polymerization of methyl methacrylate (MMA) on the fluorescence of a series of donor-acceptor molecules, [p-(N,N-dialkylamino) benzylidene] malonitriles. The extremely fast deactivation rate of the singlet excited state of these dye molecules during the early stages of the polymerization was attributed to torsional relaxation. Excimer producing dyes have also been explored (6,14).

A third type of dye, which was mentioned above, is the reactive DAA fluorophore. It was designed by Sung et al. (26) and is based on the assumption that the kinetics of the DGEBA-DAA reaction are identical to that of the DGEBA-DDS resin system. Sung et al. (26) observed significant increases in the fluorescence quantum yield, which they attributed to increases of cure products containing tertiary amine rather than to viscosity changes.

A fourth class of fluorescent dyes, explored in this work, respond to changes in the solvent polarity. General solvent effects based on electrical properties or specific effects based on chemical interactions between the fluorophore and the solvent are reflected in wavelength shifts of the fluorescence intensity maxima (27-32). As the dipole moment and the dielectric constant of the solvent increase, the trend for fluorescence spectra is a shift toward longer wavelengths, i.e., a red shift. The fluorescence spectra also exhibit the inherent time dependence of solvent dipolar relaxation. For instance, if the fluorophore were in a fluid solvent, the dielectric relaxation time of the solvent would be considerably shorter than the fluorescence lifetime. However, if the viscosity of the solvent were to increase, its dipolar mobility would decrease and the fluorophores would be forced to emit fluorescence from progressively less relaxed states (13,27,30), leading to a blue shift.

The Lippert equation (Eq. 2) is often employed to estimate general solvent effects

on the fluorophore's emission spectrum. The solvent effects are manifested by a change in the energy of the emission relative to that of the absorption, known as the Stokes' shift (30):

$$\nu_a - \nu_f = \frac{2}{hc}\left(\frac{\varepsilon - 1}{2\varepsilon + 1} - \frac{n^2 - 1}{2n^2 + 1}\right)\frac{(\mu^* - \mu)^2}{a^3} \qquad (2)$$

where h is Planck's constant, c is the speed of light in the fluid, n is the refractive index of the solvent, ϵ is the dielectric constant of the solvent, a is the radius of the sphere in which the fluorophore exists, μ^* and μ are the dipole moments of the excited and ground states of the fluorophore, respectively, and ν_a and ν_f are the wavenumbers (cm^{-1}) of the absorption and emission, respectively. For nonpolar solvents, $\epsilon \approx n^2$ and the Stokes' shift would be zero. It has been observed that correlation of spectral positions and Stokes' shifts with macroscopic properties of solvents is not always appropriate (28). Fluorophores containing polar functional groups may partake in specific interactions, and if present, are normally the dominant factors determining absorption and fluorescence wavelength maxima of the fluorophores (18,28). Specific interactions are not accounted for by the Lippert equation, Eq. (2).

Lin and Wang (31) measured the Stokes' shift of a polarity-sensitive fluorescent probe, 1-(4-dimethylaminophenyl)-6-phenyl-1,3,5-hexatriene (DMA-DPH), as a function of the cure time of an epoxy/amine system using a conventional fluorometer. Although they observed only a 25 nm shift in the emission wavelength maximum during the course of the polymerization, they were still able to demonstrate the usefulness of polarity-sensitive fluorescent probes for cure monitoring of epoxy resins. As expected, a decrease in the Stokes' shift was observed as a function of time during cure at several temperatures. They attributed this decrease to changes in polarity as a result of the chemical reactions rather than to changes in viscosity or free volume, based on a mechanism of dielectric relaxation suggested by Pogany (32). Wang and Lowry (27) later examined a polarity-sensitive zwitterion, N-(3 sulfopropyl)-4-(p-didecylaminostyryl)pyridinium (di-10-ASPPS), which exhibited a wavelength shift of approximately 45 nm during polymerization.

Schwab and Levy (13) studied the physical aging process of amine-cured epoxies using the fluorescent dye, 4-(N,N-dimethyl amino)-4'-nitrostilbene (DMANS). This dye was found to be sensitive to changes in both the mobility and polarity of the local environment as a function of cure time. After postcuring, the emission wavelength maxima of DMANS remained constant with physical aging time, while the fluorescence intensity increased monotonically during physical aging. It is important to note that the fluorescence

measurements were made with a conventional fluorometer (13).

In the work reported herein the DMANS fluorophore was used since it displays a large fluorescence wavelength shift as the resin cures. This eliminates the need for an internal standard that is required in intensity measurements (13,18). Evanescent wave fluorescence sensing was achieved using an economical optical fiber sensor that consisted of lead oxide doped glass material with an index of refraction of approximately 1.62. The refractive index of typical glass optical fibers is roughly 1.46, whereas the refractive index of epoxy resins increases from about 1.48 to 1.58 during cure (6).

EXPERIMENTAL

Spectroscopy - Equipment & Materials

An optical bench was constructed for the cure monitoring experiments. The optical bench (Figure 2) included an Ar^+ laser (Spectra Physics Series 2000*), beam directing mirrors, a beamsplitter (microscope slide cover slip), a 40X microscope objective with a numerical aperture of 0.75, a focusing lens, a 1/8 m monochromator (Oriel, 77390), two cut-on wavelength filters, a photomultiplier detector (Oriel, 77348), and a 100 μm lead silicate optical fiber. The accompanying electronics consisted of a fast preamplifier, a photon counter, a high voltage power supply, a two axis stepper motor driver with TTL interface, and a computer. The fluorescence signal is collected at the proximal end of the fiber, into which the excitation light is coupled, significantly reducing the background compared to detecting fluorescence at the distal end of the fiber (6,18,22). The microscope objective, which focusses the excitation light into the optical fiber, was selected to have approximately the same numerical aperture as the fiber. Glass and coworkers (24) described the importance of numerical aperture on the signal generated by the fluorescent probes and of matching the optical system numerical aperture to the optical fiber's numerical aperture. The optical fiber, which was developed at NIST, contains the following mass fractions of compounds: 46.0% SiO_2, 45.3% PbO, 5.6% K_2O, 2.5% Na_2O, and 0.6% R_2O_3, where R represents the remaining materials (33).

One of the fluorescent dyes used (18,27) in this investigation (Figure 3a) was a zwitterion, called N-(3-sulfopropyl)-4-(p-didecylaminostyryl)pyridinium, abbreviated di-10-ASP-PS (Molecular Probes). Another dye used in this study (Figure 3b) was 4-(N,N-dimethyl amino)-4'-nitrostilbene (DMANS, Fisher Scientific). The salient feature of both dyes is their strong response to the polarity of their environment. Rhodamine B, a common

laser dye, was employed for calibration purposes. A commercial epoxy resin system, Tactix 123 (DOW Chemical, Figure 4a) and Jeffamine D400 curing agent (Texaco, Figure 4b), was used for all of the experiments.

Preliminary experiments were performed to demonstrate the evanescent wave fluorescence sensor as an effective cure sensor and to compare these results with fluorescence cure monitoring data obtained by other sensing geometries. Three types of fluorescence experiments were conducted using neat resin samples: one utilizing an evanescent wave sensor, the second employing a distal sensor, and finally, bulk fluorescence measurements were made with a conventional fluorometer (ISS, K2 multifrequency phase). The resin samples monitored on the optical bench were cured in a miniature aluminum cell equipped with a cartridge heater.

Sample preparation involved dissolving a relatively low concentration of one of the fluorescent probes in the Tactix 123 diglycidyl ether of bisphenol A (DGEBA) resin. $1 \cdot 10^{-4}$ mol·L^{-1} of di10ASP-PS (MW=598.93) or $1 \cdot 10^{-3}$ mol·L^{-1} of DMANS (MW=268) were added to samples cured on the optical bench, while concentrations of $1 \cdot 10^{-5}$ mol·L^{-1} or $1 \cdot 10^{-4}$ mol·L^{-1} were added to fluorometer samples, respectively. Just prior to an experiment, the doped DGEBA was mixed stoichiometrically with the Jeffamine D400. The system was stirred for several minutes under a nitrogen atmosphere at room temperature and was then degassed. The samples were subsequently placed in the preheated sample chamber of the fluorometer or fiber optic cell. The excitation wavelength of the fluorometer was held constant at 488 nm to match a commonly used Ar^+ laser line. In the case of the measurements obtained with optical fibers on the optical bench, the fluorescence intensity was measured by counting the number of photons in each spectral element that impinged on the photomultiplier tube (PMT) detector in 0.1 s. The slit width of the monochromator was 0.4 mm and the voltage on the photomultiplier tube was -1000 V.

The fluorescence measurements were correlated with infrared (IR) measurements to produce a calibration of the degree of cure with the peak position of the fluorescence spectrum. IR spectra were obtained with a Nicolet Magna 550 Fourier transform infrared (FTIR) spectrometer equipped with a mercury-cadmium-telluride (MCT-A) detector. The epoxy resin was placed between two potassium bromide plates mounted in a heated cell. The same batch of resin was used in the infrared experiments as used in the fluorescence experiments for consistency.

The plates were placed in a heated transmission cell at various isothermal temperatures, and spectra were taken periodically. Each FTIR spectrum consisted of eight

co-added interferograms at 4 cm^{-1} resolution. The disappearance of the oxirane or epoxide peak at 970 cm^{-1} was monitored and the aromatic hydrogen in-plane deformation at 1184 cm^{-1} was chosen as the reference peak (34). The oxirane conversion, α, was then calculated using the following equation:

$$\alpha = 1 - \frac{A_{970}(t)/A_{1184}(t)}{A_{970}(0)/A_{1184}(0)} \quad (3)$$

where A_{970} is the area of the oxirane peak centered at 970 cm^{-1} and A_{1184} is the area of the reference peak at 1184 cm^{-1}. The ratio at time equal to zero, $A_{970}(0)/A_{1184}(0)$, was obtained from a spectrum of an uncured sample at room temperature. A few minutes were required to place the specimen between the KBr plates and for the epoxy sample to reach its cure temperature. Therefore, it was necessary to estimate the elapsed cure time, which was accomplished by extrapolating back to the initial normalized absorbance obtained at room temperature. Additionally, it should be noted that a reference spectrum of the preheated blank plates was obtained prior to each experiment.

Liquid Molding

Liquid molding experiments with the optical fiber embedded in a glass fiber preform were performed using a resin system doped with the DMANS fluorophore. As in the preliminary experiments the fluorescent dye was dissolved in the Tactix 123 DGEBA epoxy at a concentration of $1 \cdot 10^{-3}$ $mol \cdot L^{-1}$. In the present experiments the optical fiber was not woven into the fiber preform. Rather the fiber reinforcement and optical fiber were positioned in the mold with the optical fiber sensor conveniently placed through the center of the reinforcement. The edges of the mold were sealed with adhesive/sealant to prevent edge effects during the resin injection.

Parts were molded in a flat plaque mold indicated in Figure 5. The top and bottom platens of the mold were cast aluminum and contained cast-in electrical heating elements and cooling tubes (Watlow custom design). The platens also contained bayonet fittings to support the resistance temperature devices (RTD's) used to measure the platen temperatures. A thin film RTD (Omega F3105) was mounted in the center of the preform to provide a direct measurement of the center temperature of the molded part during processing. One of the RTD signals was used as the process variable in a stand alone temperature controller (CVL Instruments) that varied the electrical power supplied to the platen heating elements for control of the temperature setpoint. All temperature measurements were forwarded to a computer (50MHz i486DX) via a signal conditioner (Omega OM5) to allow the use of the

measured temperatures in higher level calculations. The controller permitted the temperature setpoint to be downloaded from the computer, thereby allowing for complex cure cycles that could be determined on-line by a higher level controller running in the computer.

The injection system consisted of a pressurized container to feed resin to the mold and a vacuum pump (Trivac D2A) for degassing the resin and maintaining pressure control in the mold during injection. Both mold inlet and outlet pressures were measured with pressure transducers (Omega PX603) and controlled independently with stand alone controllers. Pressure control was achieved at the mold inlet, for example, by varying the pressure in the resin feed container. A 3-way solenoid valve connected the resin feed container to both a high pressure source (N_2 cylinder) and a low pressure source (vacuum pump). By manipulating the solenoid valve between the high and low pressure sources, the pressure in the container and at the mold inlet was adjusted to the desired set point. The pressure setpoints of the controllers could be downloaded from the computer enabling complex injection strategies designed to minimize void formation.

The composite parts consisted of Knytex D155 unidirectional glass fabric impregnated with Tactix 123 and Jeffamine D400 curing agent doped with the fluorescent probe. Prior to its injection into the mold, the resin was degassed for approximately ten minutes. The parts were molded with a fiber volume fraction ranging from 49.7% to 54.3%. The measured permeability of the reinforcement was roughly $9.0 \cdot 10^{-8}$ cm^2 in the direction of flow during injection when the fiber tows were oriented perpendicular to the flow direction. The permeability, which is a physical property of the reinforcement, determines the relationship between the resin injection rate and the required pumping pressure (35).

Liquid molding experiments were conducted by specifying an injection and temperature sequence; a typical sequence of gauge pressure and temperature setpoints are displayed in Figure 6. The pressure setpoints at time zero define the resin degassing conditions. The gauge pressure setpoints at time zero were set to -103kPa and maintained for approximately 10 min to accomplish degassing. A computer timer was then started which controlled the progression of the injection and temperature cycles. As shown in Figure 6, the mold inlet gauge pressure, P_i, was increased from -103kPa to 103 kPa during a period of 20 s, and the mold outlet gauge pressure, P_o, was maintained at -103kPa. After 5 min, both the mold inlet and outlet gauge pressures were changed to 97 kPa holding pressure, thereby stopping the flow.

RESULTS & DISCUSSION

Sensor Development

Evanescent wave sensing was first demonstrated with Rhodamine B, which was also used to calibrate the optical system (36). Rhodamine B was dissolved in propylene glycol at a concentration of $1 \cdot 10^{-4}$ mol·L^{-1}. The fluorescent dye was excited at 488 nm and its peak fluorescence was observed at 580 nm. A series of experiments were conducted in which assorted lengths of the optical fiber were immersed in the dye solution, and in accordance with theory (6,36), the fluorescence intensity was observed to be a linear function of the exposed fiber length.

The next phase of the project entailed testing fluorescent dyes that respond to physical changes in curing epoxy resins. The two polarity-sensitive fluorescent dyes, di-10-ASP-PS and DMANS, were examined for use in the Tactix 123/Jeffamine D400 system. The intensity of naturally occurring fluorescence by the Tactix 123/Jeffamine D400 system itself was nominal, which eliminated the need to resolve overlapping fluorescence emission peaks upon addition of either fluorescent probe. It is important to note that the resins used were industrial-grade resins, rather than purified scientific-grade resins which are often employed for sensor demonstration.

Emission spectra were obtained as a function of time at 50 °C, 60 °C, and 80 °C for both resin/dye systems using a conventional fluorometer, in the wavelength range between 495 nm and 700 nm. The di-10-ASP-PS exhibited shifts of approximately 45 nm, while the DMANS displayed shifts between 65 nm and 70 nm. The use of frequency shifts obviates the need for an internal standard, as is required with probes whose fluorescence intensity is sensitive to degree of cure. Another advantage to using a wavelength-shift probe is that peak frequencies are less dependent on the signal-to-noise ratio than intensities.

As described earlier in the paper, the extent of cure was calibrated to the fluorescence wavelength-shifts by monitoring the mid-infrared spectrum obtained by FTIR spectroscopy. Thus, the sole purpose for developing the calibration curve was to demonstrate the methodology of the cure monitoring technique. The FTIR experiments were conducted under the same conditions as the fluorometer measurements. The correlation of the peak shift from the fluorescence probe with the degree of cure from the IR data is illustrated in Figure 7 for the DMANS probe at temperatures of 70 °C, 90 °C, and 110° C. A time correction was made to the infrared data to account for the monomer conversion that occurred during sample placement and preheat, and was described in the previous section. However, a similar correction was not made to the fluorescence data. The sample loading time for the fluorometer experiments was short compared to the FTIR experiments.

The wavelength of the maximum in the fluorescence intensity shifted significantly during the course of isothermal cures at various temperatures. The infrared data on the resin system was collected at identical temperatures and the degree of cure computed with Eq.(3). As the Lippert equation (Eq. 2) predicted, λ_{max} decreased with decreasing monomer concentration (Figure 7), due to changes in the refractive index and dielectric constant of the curing resin.

To determine the suitability of the probe molecules for in-mold cure monitoring, evanescent wave and distal mode experiments were conducted for both fluorescent dyes, and these optical fiber based measurements were compared to the fluorometer measurements. Noise in the optical fiber spectra was smoothed by subtracting the background spectrum and performing a cubic spline fit of the data (37,38) to obtain the wavelength of the peak maxima. Figure 8 shows the evolution of peak maxima with time from fluorometer, distal and evanescent wave measurements. The blue shift produced by the di-10-ASP-PS probe was significantly smaller in the evanescent wave mode than in the fluorometer (Figure 8a), and this observation was reproduced in several experiments. Most importantly, the fluorescence maximum at time zero in evanescent wave mode was very different from distal mode or bulk mode in the case of di-10-ASP-PS, but not for DMANS. A possible explanation is that a fast surface interaction occurred between the highly polar zwitterions and the glass fiber, causing the evanescent wave sensor to lose sensitivity to the physical changes occurring in the epoxy resin. The DMANS probe however, exhibited large wavelength shifts with the evanescent wave sensing system as well as in the fluorometer and the distal mode (Figure 8b). The scatter in the optical fiber results are attributed to thermal inaccuracies in the heated cell owing to the simplicity of the cell design. However, since the performance of the DMANS fluorophore clearly exceeded that of the Di-10-ASP-PS probe in the evanescent wave sensing geometry, only the DMANS probe was used for in-mold monitoring.

In-Mold Monitoring

Figure 9 illustrates a typical fluorescence spectrum obtained during a LCM experiment conducted according to the cure schedule shown in Figure 6. In this experiment, a composite plaque was produced with 52% by volume glass fiber. The spectrum consists of a single broad peak, and accurate determination of the peak location requires smoothing the data. Note that the current equipment produces a spectrum from only one scan of the wavelength range taken in 3 minutes. An improved system uses a CCD camera to decrease

the data acquisition time and to produce higher signal-to-noise ratio by allowing for signal averaging. A plot of the peak maximum wavelength, λ_{max}, as a function of time, is given in Figure 10 for the experiment from which the spectrum in Figure 9 was taken. Once the fluorescence signal is obtained, smoothed, and the peak maximum found, the degree of cure is obtained from the previously developed correlation with FTIR data, illustrated in Figure 7.

A number of molding experiments have been performed to demonstrate the ability of the evanescent wave fluorescence sensor to follow the resin cure in the mold, and a summary of these experiments is presented in Table 1. Four parameters were varied, including driving pressure, outlet pressure, temperature, and fiber volume fraction to evaluate the accuracy and range of operation of this monitoring technique. It was observed immediately that void-free composites could not be produced at isothermal molding temperatures higher than 100 °C. As a result, no usable cure data was obtained at these higher temperatures.

Figures 11a and 11b exhibit the Stokes' shift as a function of time for several liquid molding experiments conducted at 70°C and 90°C, respectively (Table 1). The Stokes' shift was plotted instead of λ_{max} to more closely match the Lippert equation, however the general shapes of the curves are the same if either λ_{max} or Stokes shift is plotted. The Stokes' shift was calculated by expressing the fluorescence wavelength maxima in terms of frequency, which was subtracted from the excitation frequency. In this experiment, a laser excitation source was used, therefore the excitation frequency was held constant. The traditional method for computing the Stokes' shift requires the excitation wavelength maxima to be measured along with the emission wavelength maxima.

Another important issue that had to be addressed before these plots could be constructed was how to devise a method for computing time equal to zero, since it was unknown. The details concerning how time equal to zero was defined are discussed below.

Preliminary Data Analysis

Two different types of mold spacer plates were used for the series of liquid molding experiments conducted. One design allows the fiber to be positioned across the center of the mold, while the other spacer plate has two sets of ports which are equidistant from each other and the inlet and outlet ports, respectively. When the second mold frame was used, the fiber was placed in the slot closer to the outlet port. With this information as well as knowledge of the mold filling times for each of the experiments, one could estimate when the resin first made contact with the optical fiber, assuming the flow front advanced uniformly

through the mold.

Practice has converged on the use of Darcy's law to describe the impregnation of the resin in the mold containing the preforms (39). The following relationship may be extracted when the pressure driving the flow is held constant and the flow is isothermal

$$x^2 = kt \tag{4}$$

where x represents the flow front position, t is time, and k represents a constant. For example, the optical fiber wetout time for experiment "DWJS29" was calculated to be 91 s after mold filling was initiated with Eq. (4). The mold was filled after 205 s and since the mold frame containing two sets of ports was used for this particular experiment, the following calculation was made: (205 s) x $(2/3)^2$ = 91 s. A summary of the mold filling times for each of the liquid molding experiments, as well as the estimated fiber wetout times for each can be found in Table 2. Although Eq. (4) assumes that the resin was at a constant temperature during injection, this was not the case since the resin was at room temperature when it was injected into the preheated mold. However, the necessary corrections that would have to be made to Eq. 4 are beyond the scope of this paper, and interested readers should refer to other references (40).

After the resin arrived at the outlet port, the resin flow was allowed to continue for a period of time to insure adequate infiltration of the preform and to prevent void formation upon increasing the outlet pressure. Therefore, the times at which the resin flow was curtailed during each of the experiments was recorded and is also presented in Table 2. In order to simplify this analysis, it was assumed that after mold filling the resin surrounding the optical fiber was composed entirely of freshly injected sample. In reality, Taylor dispersion might have played a significant role during the injection stage (40), which would suggest that the sample about the fiber optic was of a variety of ages.

Elapsed time was therefore corrected by adding the time after which the resin flow was stopped from the mold filling time, plus the estimated fiber wetout time in each of the experiments. Or alternatively,

$$Tc = TRFS - MFT + EFWT \tag{5}$$

where Tc represents the time correction, TRFS is the time the resin flow was stopped, MFT is the mold filling time, and EFWT is the estimated fiber wetout time (Table 2). Therefore the following correction was made to the elapsed time values:

$$t' = t - Tc \quad (6)$$

where t represents uncorrected or raw elapsed time and t', corrected elapsed time. The time-corrected results are displayed in Figures 11a and 11b. For example, in "DWJS26" (Figure 11b) the filling time (MFT) was 1390 s and the resin flow was stopped (TRFS) after 3090 s. The difference between these values were then added to the estimated fiber wetout time (EWFT), 618 s. Therefore, in this particular experiment the corrected time equal to zero (t' = 0) would correspond to t = 2318 s.

The extent of cure during liquid molding of the composite plaques was extracted from Figures 11a and 11b using the calibration curve of the wavelength shifts to remaining monomer (Figure 7). Sample cure curves at each temperature are presented in Figure 12.

Determination of Uncertainty

An error analysis was carried out to explain the scatter in the fluorescence time profiles (Figures 11a & 11b). Although the data at each temperature were not obtained under identical experimental conditions (see Table 1), the data sets were analyzed collectively. One of the purposes of the error analysis was to assess which processing variables had contributed most to the variation in the data. The observed parameters included elapsed time during cure, outlet pressure, driving pressure, number of layers, mold filling time, time the resin flow was stopped, and the estimated fiber wetout time.

Prior to performing the error analysis, a good model for the data in Figures 11a and 11b had to be obtained, and the fitting was accomplished using the statistical software package, Dataplot (41). Both the 70°C and 90°C data were modeled using a quadratic spline fit, and were naturally fitted separately (Figures 13a & 13b). The quality of each fit was determined by the pooled standard deviation of all of the data points, S_{res}, and by the structure of the residuals (41). Ideally, S_{res} should be small (i.e., approaching intrinsic instrument variation) and the residual plots should be structureless, indicating that all of the deterministic content of the data has been accounted for by the model.

For the 90 °C data, the residuals of the quadratic spline fit were plotted as a function of each of the variables listed above. When the quadratic spline residuals were plotted as a function of elasped time (Fig. 14a), the plot was not completely structureless, which suggested that the model could be improved. Figure 14a also revealed that the magnitude of the error was highest at low "elapsed time" values. Analysis of the other variables revealed little information, which suggested that their contribution to the global uncertainty was relatively small compared to the elapsed time.

A typical underlying assumption in any "least squares" fitting process is that the intrinsic standard deviation, σ, is constant for all data points, that is, all of the data points are equally precise. If not, the resulting fitted model may be improved further by providing information to the fitting process that reflects the model quality (i.e., σ of each data point). Figure 14a portrays a non-constant bandwidth of residuals, indicating that the data at earlier times were intrinsically less precise than the data collected at later times for the composite parts processed at 90 °C. This being the case, the variation in precision would have to be estimated and incorporated into the fitting procedure, in order to improve the quality of the fit via weighted least-squares fitting. Nonetheless, "elapsed time" was discretized and individual values for σ were calculated for each region (Fig. 15a). As Figure 15a illustrates, σ ranged from 300 cm^{-1} during the early stages of cure to 38 cm^{-1} during the latter stages of cure for the 90 °C data (Fig. 14a). If Fig. 11a were plotted in terms of λ_{max} rather than Stokes Shift, the range of σ would be between 12 nm and 1.3 nm, respectively.

A similar analysis of the uncertainty was performed on the 70 °C data (Figs. 14b & 15b). The plot of the quadratic spline residuals as a function of the elapsed time does not possess the structure observed in Figure 14a. Instead, the relationship between the variables appears essentially homogeneous. Figure 15b, which displays σ as a function of discretized "elapsed time" values, suggests a decrease in σ with elapsed time, however this trend is not nearly as dramatic as the one depicted in Figure 15a. A possible explanation for this behavior is that good time resolution was less critical at the lower processing temperature, since the resin cured much more slowly at 70 °C than at 90 °C. Therefore, with regard to the 70 °C data, initial values of σ were not as high for the data points acquired earlier in time, as compared to the data collected at 90 °C (Fig. 15a). The reader should also be reminded that the values for σ depicted in Figure 15b are based on fewer observations than those presented in Figure 15a. As illustrated in Figure 15b, values for σ ranged between 25 cm^{-1} and 170 cm^{-1}, or alternatively, between 1.1 nm and 7.2 nm (with respect to λ_{max}).

The portion of the uncertainty in the measurements that could be attributed to instrumentation error was also estimated. The instrument error in the measurement of λ_{max} was calculated by taking the product of the diffraction grating dispersion and the monochromator slit width. The dispersion of the 1200 lines/mm diffraction grating was 6.5 nm/mm and the slit widths of the monochromator were set at 0.4 mm. The size of the spectral element was therefore 2.6 nm and the uncertainty in the spectral reading was ±1.3 nm. Note that the standard deviation in the measurements declined to approximately 1.3 nm during the latter stages of the experiments.

As shown by the analysis of the uncertainty, the main source of error was the poor time resolution of the instrumentation. It was introduced by the fact that the required data acquisition or scan time was as long as three minutes. If a faster data acquisition system were implemented, it is expected that the uncertainty in the fluorescence measurements would be significantly smaller. One might accomplish this by replacing the monochromator and PMT with an imaging spectrograph and a CCD array camera. Perhaps a better estimate of time equal to zero could also be obtained by referencing cure measurements obtained during liquid molding against measurements acquired in a temperature-controlled cell. Additionally, it is probable that the pursuit of a more rigorous flow analysis (40), such as the one described above, would lead to a better estimate of time equal to zero.

Fluctuations in the signal-to-noise ratio (SNR) introduced another source of uncertainty in determining λ_{max}. Changes in SNR during the course of a scan would have perturbed the measurement of λ_{max}. In general, the SNR was relatively low at the beginning of a cure monitoring experiment, and would improve significantly over time. Finally, the SNR would level off or decrease moderately. No relationship was observed between σ and SNR itself, since σ was clearly dominated by the poor time resolution of the instrumentation and by the error in estimating time equal to zero in each of the experiments.

A possible explanation for the observed trend in SNR is as follows. During the early stages of cure, the resin viscosity is relatively low. Fluorophores are then most apt to expel their energy by nonradiative means, and as a result, only a small population of fluorescent dye molecules will emit radiation. As the resin viscosity increases, the molecular rotation of the dye molecules become progressively more hindered by the presence of potential energy barriers (42). Therefore, the SNR would be expected to increase during the course of cure. However, the SNR normally stopped increasing after gelation, when the mobility of the fluorophores became negligible. This behavior was assumed to be a consequence of photobleaching of the fluorophores by the excitation source (6). Although photobleaching was minimized by blocking the laser beam between scans, it could not be completely avoided due to the long scanning periods. After gelation only a limited number of fluorescent dye molecules are able to diffuse in and out of the sensing region, therefore photobleaching would be most apparent during this period.

Another factor that impacted the SNR was the length of the optical fiber that extended outside of the mold, and served as an interface with the optical bench. Although the fiber length would remain constant during an experiment, longer lengths of the uncladded fiber tended to increase the level of noise in the signal. Therefore, the length of fiber between

the mold and the optical bench was minimized. Moreover, longer lengths of fiber led to greater signal losses. It is possible this matter can be addressed in the future by applying a cladding to certain portions of the optical fiber sensor.

Chemical Analysis

Although a number of issues must be addressed before the evanescent wave fluorescence sensor (EWFS) can be employed in a manufacturing environment, the above analysis demonstrated the feasibility of the EWFS cure monitoring technique. In fact, the uncertainty in fluorescence measurements obtained towards the end of cure approaches the error in the instrument reading itself. The reliability of λ_{max} towards the end of cure proved useful in a different context as well. The cure sensor alerted the authors to disparities between two batches of Tactix 123/Jeffamine D400, one of which had degraded quite significantly. It had repeatedly been observed that in the older batch of resin, λ_{max} would approach 580 nm at the end of cure, while in the newer batch of resin, λ_{max} only converged to 590 nm.

Differences in the λ_{max} shifts, as well as in the monomer conversion data were also observed. Figure 16 depicts the correlation of remaining monomer vs. λ_{max} for the older batch of resin, which can be compared with the correlation obtained for the newer batch of resin (Figure 7). Although the cure data used in each calibration were obtained at different temperatures and therefore cannot be compared directly, the overall shapes of the curves are markedly different. It is important to note that poor time resolution was also a source of error during the development of the calibration plots, since the fluorometer utilizes a monochromator and PMT.

Nevertheless, efforts were made to explain these observed differences by testing both resin systems for degradation and water sorption. Both sets of Tactix 123 and Jeffamine D400 samples were analyzed using a Hewlett-Packard gas chromatograph-mass spectrometer (GC-MS) model 5971. Amine samples were prepared by dissolving a few microliters of the diamine into a few milliliters of derivatizing reagent, methyl-bis-trifluoroacetamide. It was necessary to cap one of the amine hydrogens to help prevent the diamine sample from adsorbing onto the GC column. Epoxy samples were prepared by dissolving a few microliters of epoxy into a few milliliters of methylene chloride. After injection, the sample was held at 100°C for two minutes and was subsequently ramped to 280°C at 15°C/min.

Figures 17a and 17b illustrate the GC traces for one of the fragment ions from the Jeffamine D400 (MW=154). By examining how Jeffamine D400 is likely to fragment, it is

possible that ion 154 had the structure depicted in Figure 17c. Even after the y-axis was normalized, it was evident that this species was dominant in the newer batch of diamine and the composition of the two amine samples differed significantly (43). From the GC trace, the large peaks in the newer Jeffamine material at long retention times (greater than 22 minutes) suggested the average molar mass of the newer material was higher.

Mass spectra of material eluted after 20 minutes is present in Figures 18a and 18b. These were typical mass spectra for the peaks in each lot of Jeffamine. In other words, the mass spectrum in Figure 18a was typical of the mass spectra seen for the major GC peaks from the old material, while Figure 18b was typical for the new material. For example, the fragment ion 212, was abundant in the newer Jeffamine sample but was not observed in the spectrum of the older sample.

Similar data is also furnished for both epoxy resins (Figures 19a-d). Both the gas chromatograms and the mass spectra differed dramatically from one another. The material which gave rise to the large peak in the gas chromatogram of the newer epoxy sample had evidently disintegrated in the older epoxy. Also, ions 325 and 340 appeared in the mass spectrum of the newer sample but not in that of the older sample. Ion 340 corresponds to DGEBA, and ion 325, to DGEBA less one methyl group (Figure 19b). The mass spectrum of the older epoxy sample displayed evidence of hydrolyzed DGEBA (44), and illustrations of these fragment ions are also presented (Figure 19d).

Both sets of DGEBA and Jeffamine D400 specimens were also evaluated for moisture content. The measurements of water were made by titration with Karl Fischer reagent using a volumetric titration method, modified by Margolis (45). Measurements were made on Metrohm Instruments models E547 and 633 (Brinkmann Instruments Inc.) and a water-saturated octanol solution (WSO) was used to calibrate the equipment. Additional details concerning the experimental apparatus are reported elsewhere (45).

The amine samples were titrated in pure methanol, however the epoxy samples were titrated in a 2 to 1 ratio of toluene to methanol. The addition of toluene in the latter set of samples permitted complete solubilization of the sample in the titration solvent, required for accurate determination of moisture content (45,46). The titration curve of a typical Karl Fischer titration is presented in Figure 20. The moisture content of each sample was calculated by determining the chart distance traversed during the titration of a standard of known water content (.0502 mg H_20/mg WSO) and using this to calculate the amount of water represented by the chart distance traversed during the epoxy or amine titrations (45, 46).

A summary of the results of the moisture measurements for both sets of specimens can be found in Table 3. The results revealed that the older batch of Jeffamine contained 4.4 times as much water, on average, than the newer batch. Similarly, the older batch of DGEBA contained an average of $5.2 \cdot 10^{-3}$ mg H_20 per mg of sample, while the average water content of the newer batch was $7.3 \cdot 10^{-4}$ mg H_20 per mg of sample. It is widely recognized that moisture and hydroxyl compounds will accelerate the reaction between epoxides and amine compounds (47), which would explain the differences in the curing reactions between the two batches of resin. Furthermore, it was later realized that when the older batch of DGEBA was first used, it had already exceeded its shelf life of two years (44).

The chemical analysis results also eliminated an early suspicion that the presence of water had led to an error in the interpretation of the observed λ_{max} data in the newer batch of resin. The newer diamine sample's λ_{max} values were consistently higher than the older sample's values after gelation, and such behavior would suggest that the newer DGEBA is more polar. To this end, moisture presumably had no bearing on the fluorescence signal, since the above analysis confirmed the newer samples contained far less water than the older specimens.

SUMMARY

A cure monitoring sensor has been developed based upon an evanescent wave fluorescence measurement, and was performed with an optical fiber embedded in the fiber preform reinforcement. The fluorescent dye chosen for in-mold cure monitoring was a wavelength-shift probe, DMANS, which out-performed another wavelength-shift dye, di-10-ASP-PS, when used with an evanescent wave optical fiber sensor. The decrease in the wavelength maximum of the DMANS fluorophore that occurs during cure was correlated with monomer conversion as determined by infrared spectroscopy.

The wavelength shifts were monitored during liquid molding, and the monomer conversion were later extracted from the calibration curves. The evanescent wave fluorescence sensor also proved capable of discerning problems such as resin degradation.

The optical fiber is similar in cost to standard glass optical fiber, but the addition of lead oxide raises the refractive index above that of epoxy resins, permitting evanescent wave sensing. Evanescent wave sensing allows the measurement to be obtained within approximately one micrometer radius of the fiber surface, providing a measurement of resin cure that is most appropriate for predicting final part properties.

The molding system used to make the parts with the embedded optical fiber is

designed to permit the use of the fluorescence signal in a hierarchical control strategy. The implementation of an imaging spectrograph and CCD array camera to speed data acquisition will allow the evanescent wave fluorescence sensor to be used as a cure controller, and will also result in much improved time resolution.

References

1. C. F. Johnson, in "Engineered Materials Handbook, Vol. 1, Composites", 1987. ASM International, Materials Park, Ohio.

2. D. Hunston, W. McDonough, B. Fanconi, F. Mopsik, F. Wang, F. Phelan and M. Chiang: "Assessment of the State-of-the-art for Process Monitoring Sensors for Polymer Composites", Report NISTIR 4514, U.S. Department of Commerce, June 1, 1991.

3. B. Fanconi, F. Wang, D. Hunston and F. Mopsik, in "Materials Characterization for Systems Performance and Reliability", (Eds. J. W. McCauley and V. Weiss), 275-291; 1986. Plenum Publishing Corporation, New York, N.Y.

4. D. Kranbuehl, P. Kingsley, S. Hart, G. Hasko, B. Dexter and A. Loos, Polymer Composites, 15(4), 1994, 299-305.

5. J. Mijović, F. Bellucci, & L. Nicolais, J. Electrochem. Soc., 142(40), 1995, 1176-1182.

6. F. W. Wang and B. M. Fanconi: "In-Situ Characterization of the Interface of Glass Reinforced Composites", Report NBSIR 87-3581, U.S. Dept. of Commerce, 1987.

7. G. R. Palmese, Ph.D. Thesis, University of Delaware, 1992.

8. M. A. Afromowitz, Journal of Lightwave Technology, 6(10), 1988, 1591-1594.

9. M. L. Myrick, S. M. Angel, R. E. Lyon, and T. M. Vess, SAMPE Journal, 28(4), 1992, 37-42.

10. J. F. Maguire and P. L. Talley, Journal of Advanced Materials, 26(2), 1995, 27-40.

11. J. F. Aust, K. S. Booksh, C. M. Stellman, R. S. Parnas, and M. L. Myrick, submitted to Analytical Chemistry.

12. R. L. Levy and S. D. Schwab, Polymer Composites, 12(2), 1991, 96-101.

13. S. D. Schwab and R. L. Levy, in "Advances in Chemistry Series No. 227; Polymer Characterization: Physical Property, Spectroscopic, and Chromatographic Methods", (Eds. C. D. Craver and T. Provder), 397-408, 1990. The American Chemical Society.

14. A. J. Bur, F. W. Wang, C. L. Thomas and J. L. Rose, Polym. Eng. and Sci., 34(8), 1994, 671-679.

15. H. J. Paik and N. H. Sung, Polym. Eng. and Sci., 34(12), 1994, 1025-1032.

16. W. Dang and N. H. Sung, Polym. Eng. and Sci., 34(9), 1994, 707-715.

17. P. R. Young, M. A. Druy, W. A. Stevenson and D. A. C. Compton, SAMPE Journal, 25(2), 1989, 11-15.

18. D. L. Woerdeman and R. S. Parnas, Proc. SPE ANTEC 1995, Vol. II, 2805-2811.

Society of Plastics Engineers, Brookfield, CT.

19. A. Fuchs and N. H. Sung, Proc. SPE ANTEC 1995, Vol. II, 2437-2441. Society of Plastics Engineers, Brookfield, CT.

20. N. J. Harrick, "Internal Reflection Spectroscopy", 1979, 13-33. Harrick Scientific Corporation, Ossining, New York.

21. C. K. Carniglia, L. Mandel and H. Drexhage, J. Opt. Soc. Am. 62(4), 479-486.

22. M. J. Block and T. B. Hirschfeld, "Assay Apparatus and Method", U.S. Patent 4, 558, 014, 1984.

23. J. D. Andrade, R. A. Van Wagenan, D. E. Gregonis, K. Newby and J. N. Lin, IEEE Trans. Electron Devices ED-32, 1985, 1175.

24. T. R. Glass, S. Lackie and T. Hirschfeld, Applied Optics, 26(11), 1987, 2181-2187.

25. R. O. Loutfy, Macromolecules, 14, 1981, 270-275.

26. C. S. P. Sung, E. Pyun and H. L. Sun, Macromolecules, 19, 1986, 2922-2932.

27. F. W. Wang and R. E. Lowry, "Wavelength-Shift Fluorescent Probes for Cure Monitoring of Epoxy Resins", submitted to Polymer.

28. E. L. Wehry, in "Practical Fluorescence", (Ed. G. C. Guilbault), 127-145; 1990. Marcel Dekker, Inc.

29. E. Lippert, in "Luminescence of Organic and Inorganic Materials", (Eds. H. P. Kallman and G. M. Spruch), 271-275; 1962. John Wiley & Sons, Inc., New York, N.Y.

30. J. R. Lakowicz, "Principles of Fluorescence Spectroscopy", 1983, Chapters 7 & 8. Plenum Press, New York, N. Y.

31. K. F. Lin and F. W. Wang, Polymer, 35(4), 1994, 687-691.

32. G. A. Pogany, Polymer, 11, 1970, 66.

33. D. Blackburn, Private Communication, 1994.

34. Y. Deng and G. C. Martin, Macromolecules, 27, 1994, 5147-5153.

35. D. L. Woerdeman, F. R. Phelan and R. S. Parnas, Polymer Composites, 16 (6), 1995, 470-480.

36. D. L. Woerdeman, J. P. Dunkers and R. S. Parnas, Proc. 10th Annual ASM ESD Advanced Composites Conference, 10, 1994.

37. P. Craven and G. Wahba, Numer. Math., 31, 1979, 377-403.

38. M. F. Hutchinson, ACM Transactions on Mathematical Software, 12(2), 1986, 150-153.

39. S. G. Advani, M. V. Bruschke, & R. S. Parnas, in "Flow and Rheology in Polymer Composites Manufacturing," S. G. Advani (ed.), Composite Materials Series, Elsevier, 10, Ch. 12, 1994, 488.

40. R. B. Dessenberger & C. L. Tucker, Polymer Composites, 16(6), 1995, 495-506.

41. J. Filliben, Private Communication, 1996.

42. C. P. Smyth, "Dielectric Behavior and Structure," McGraw-Hill Book Company, Inc., New York, 1955.

43. M. Welch, Private Communication, 1995.

44. G. A. Holmes, Private Communication, 1996.

45. M. A. Margolis, "The Amperometric Measurement of Moisture in Transformer Oil Using Karl Fischer Reagents," Analytical Chemistry, in press.

46. M. A. Margolis, Private Communication, 1995.

47. D. O. Bowen and R. C. Whiteside, Jr., in "Advances in Chemistry Series No. 92; Epoxy Resins", (Ed. Robert F. Gould), 48-59, 1970. The American Chemical Society.

* Identification of a commercial product is made only to facilitate experimental reproducibility and to describe adequately experimental procedure. In no case does it imply endorsement by NIST or imply that it is necessarily the best product for the experiment.

ACKNOWLEDGMENTS

The authors would like to thank Mr. Douglas Blackburn of the Ceramics Division at NIST for drawing the high index optical fibers used in this work. The authors would also like to acknowledge Dr. Bert Rust of the Applied Mathematics Division of NIST for introducing them to references 37 and 38 and for providing the corresponding computer algorithm. They would also like to thank Dr. Jim Filliben and Ms. Susannah Schiller of the Statistical Engineering Division for providing their expertise and assistance in performing the error analysis. Additionally, the authors gratefully acknowledge Drs. Michael Welch and Sam Margolis of the Organic & Analytical Chemistry Division for sharing their knowledge and resources required for the chemical analysis experiments. Finally, the authors would like to recognize Gary Spoerre of Florida State University for his technical support during the liquid molding experiments.

List of Figures

serves as an estimate of the quality of each data point. a. 90 °C data. S_{res} = 16.17486. b. 70 °C data.

Figure 16. Conversion vs. Wavelength Maximum correlation for expired epoxy/amine system at 50 °C, 60 °C, and 80 °C.

Figure 17. Gas chromatographs of Jeffamine samples to track elution times of ion 154. a. Older batch of amine. b. Newer batch of amine. c. Possible molecular structure of ion 154.

Figure 18. Mass spectra of Jeffamine samples at 20 min. a. Older batch of amine. b. Newer batch of amine.

Figure 19. Gas chromatographs and mass spectra of epoxy samples. a. Gas chromatograph of newer epoxy sample. b. Mass spectrum of newer epoxy sample at average of 20.4 min to 21.5 min. c. Gas chromatograph of older epoxy sample. d. Mass spectrum of older epoxy sample at 19.1 min to 19.5 min.

Figure 20. Typical Karl Fischer volumetric titration curve of moisture in WSO.

List of Tables

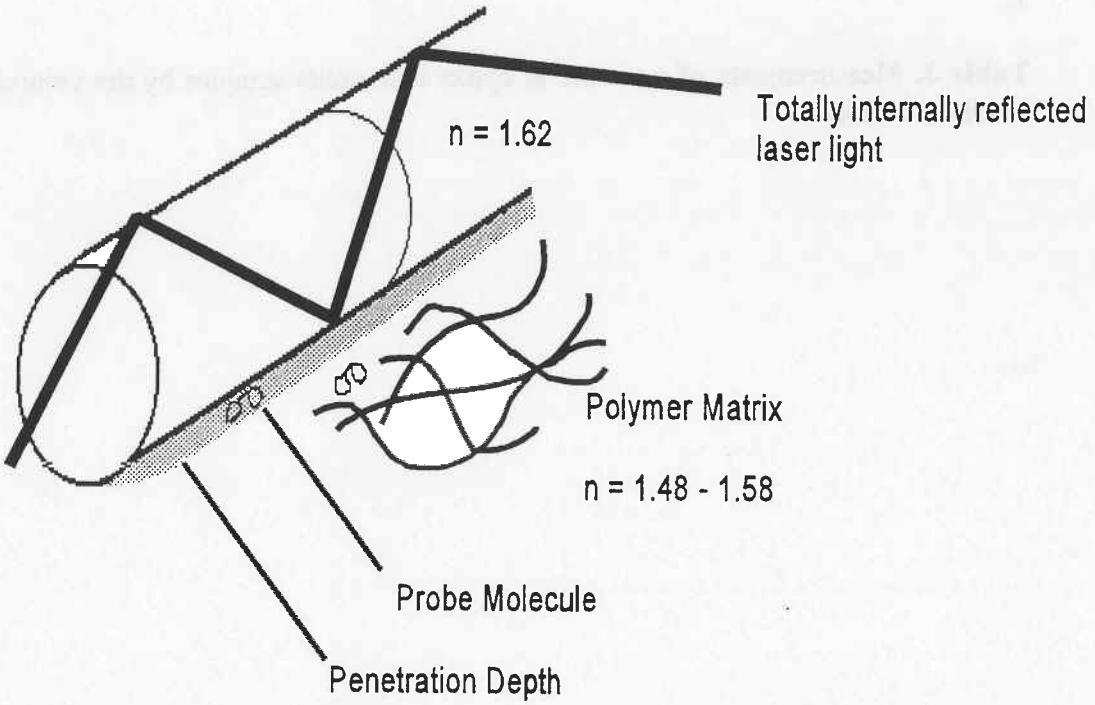
n = 1.62
Totally internally reflected laser light
Polymer Matrix
n = 1.48 - 1.58
Probe Molecule
Penetration Depth

Figure 1.

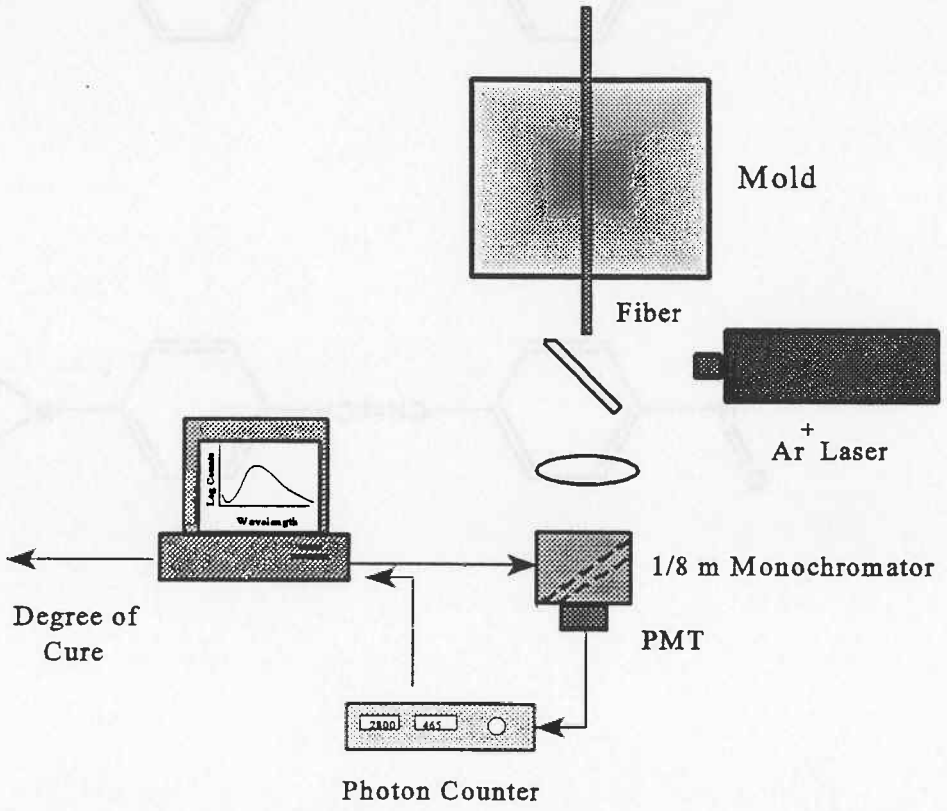
Mold
Fiber
Ar+ Laser
Log Counts
Wavelength
1/8 m Monochromator
Degree of Cure
PMT
Photon Counter

Figure 2.

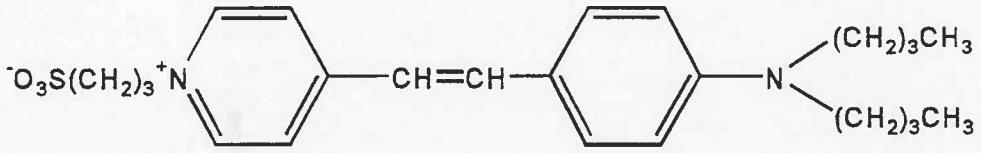

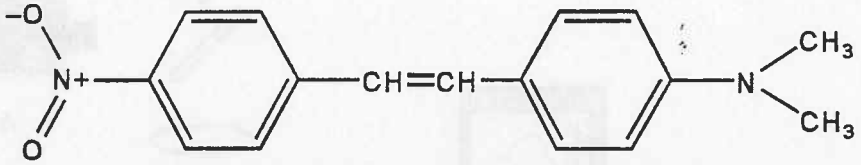

Figures 3a. & 3b.

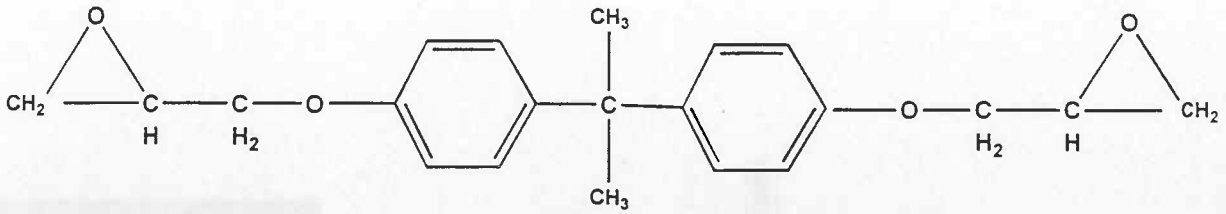

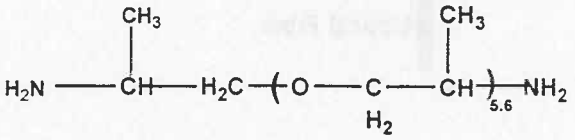

Figures 4a. & 4b.

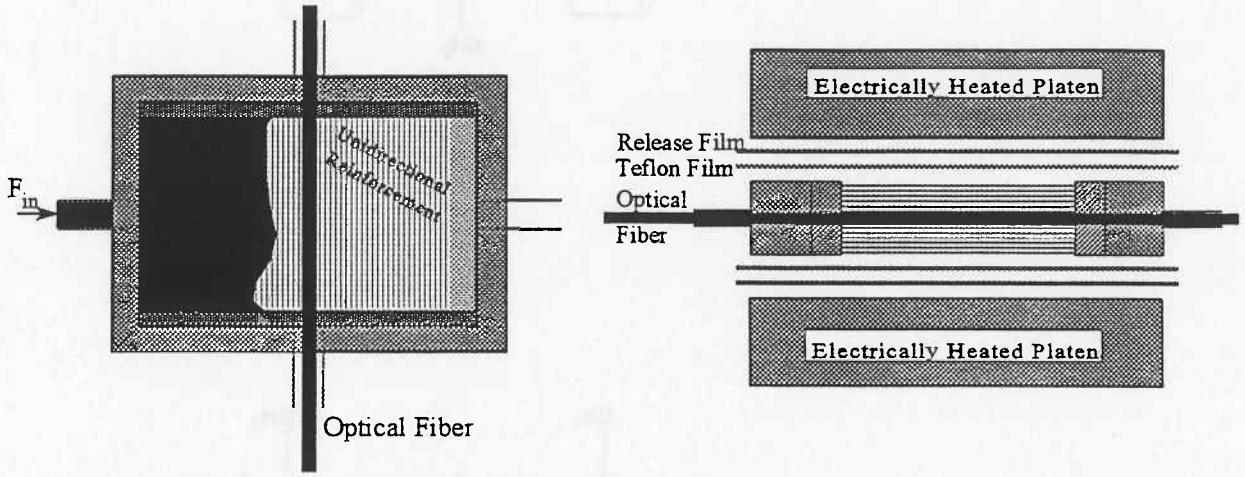
Unidirectional Reinforcement
F_{in}
Optical Fiber
Electrically Heated Platen
Release Film
Teflon Film
Optical
Fiber
Electrically Heated Platen

Figure 5.

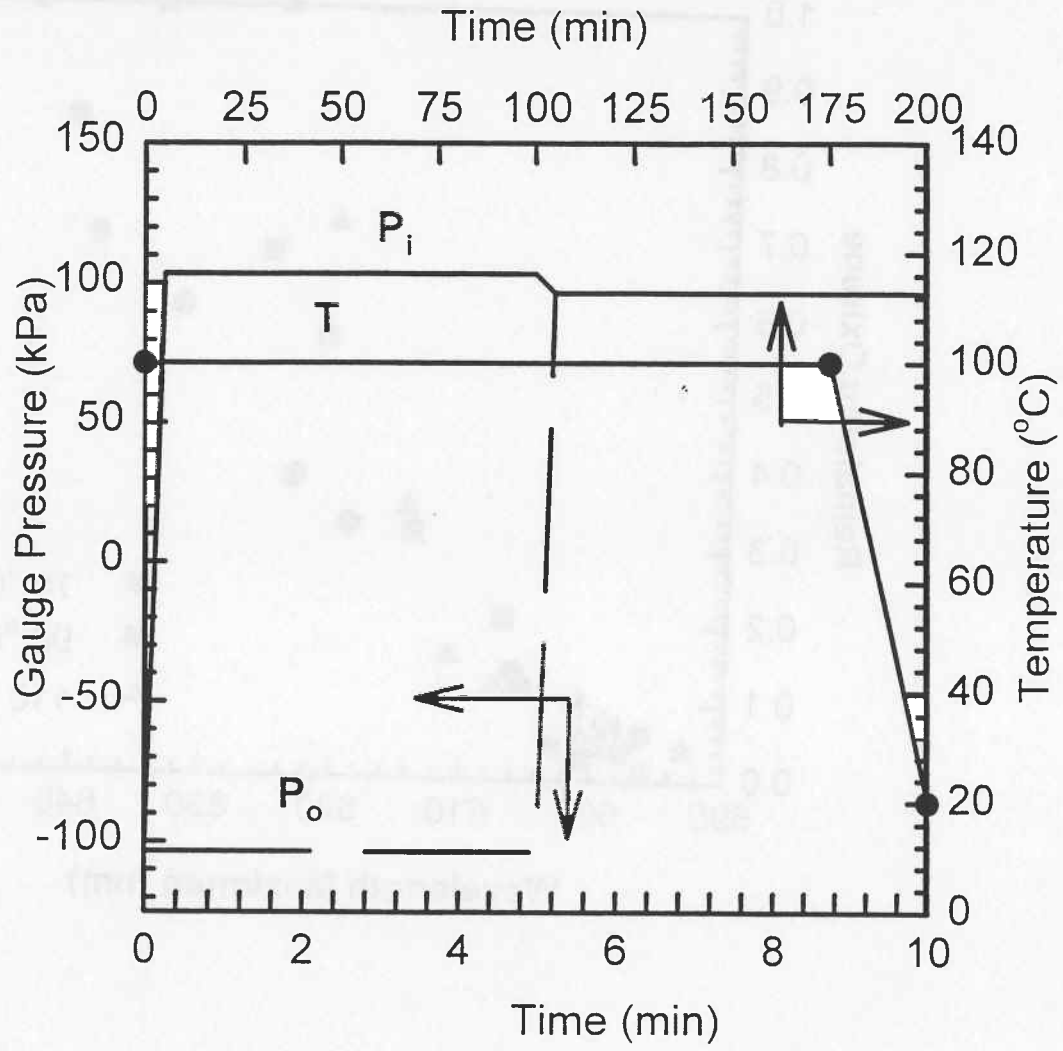
Time (min)
0
25
50
75
100
125
150
175
200
150
100
50
0
-50
-100
140
120
100
80
60
40
20
0
Gauge Pressure (kPa)
Temperature (°C)
P_i
T
P_o
0
2
4
6
8
10
Time (min)

Figure 6.

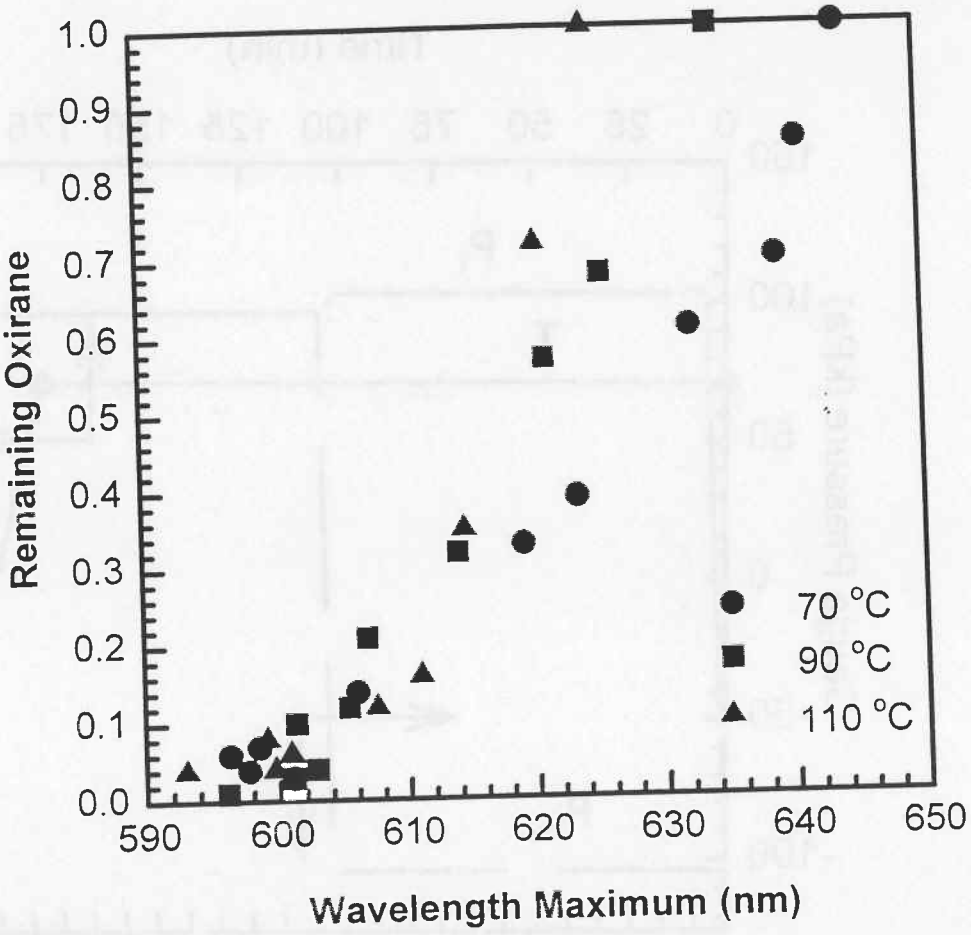
1.0
0.9
0.8
0.7
0.6
0.5
0.4
0.3
0.2
0.1
0.0
Remaining Oxirane
590
600
610
620
630
640
650
Wavelength Maximum (nm)
70 °C
90 °C
110 °C

Figure 7.

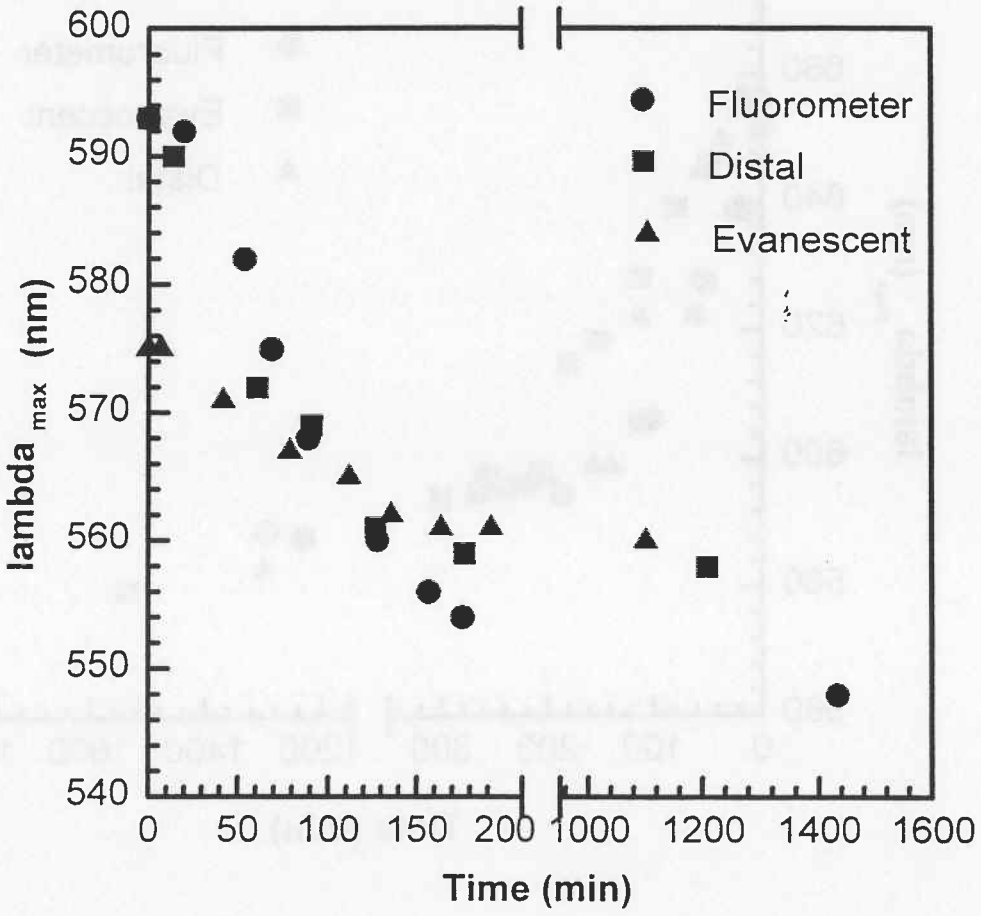
600
590
580
570
560
550
540
lambda max (nm)
0
50
100
150
200
1000
1200
1400
1600
Time (min)
Fluorometer
Distal
Evanescent

Figure 8a.

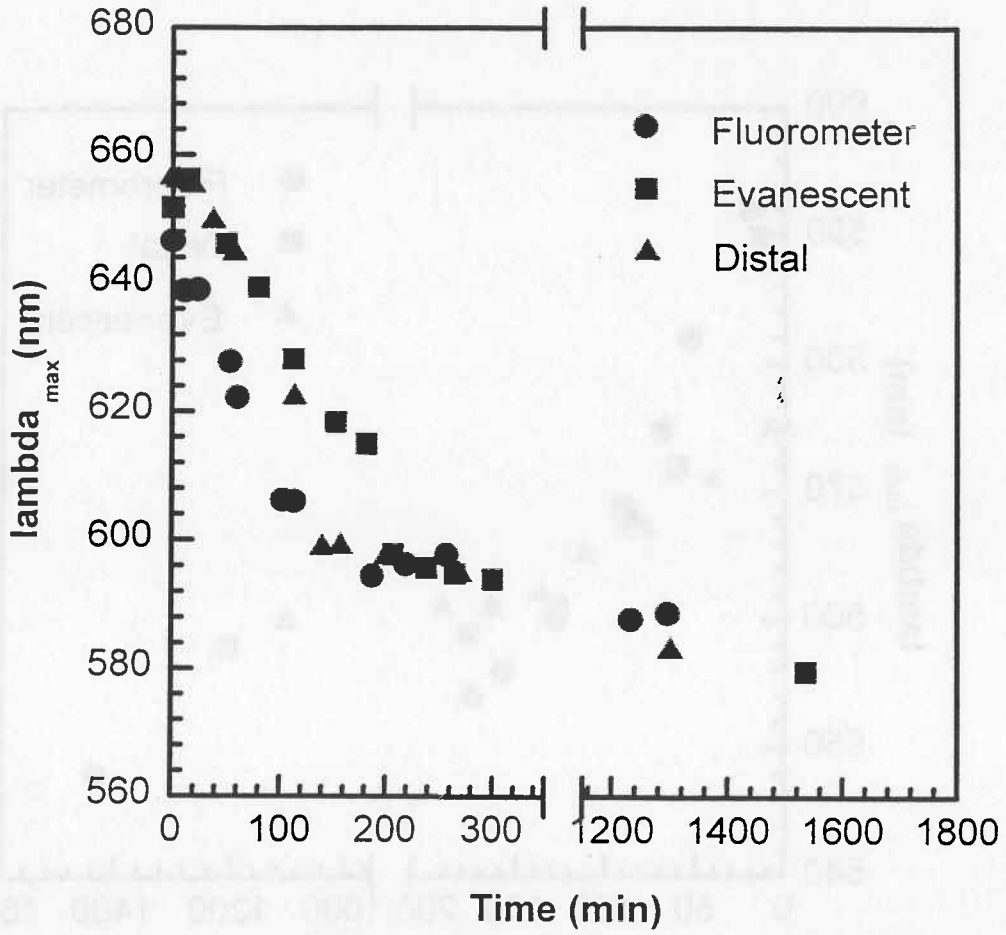
680
660
640
620
600
580
560
lambda max (nm)
0
100
200
300
1200
1400
1600
1800
Time (min)
Fluorometer
Evanescent
Distal

Figure 8b.

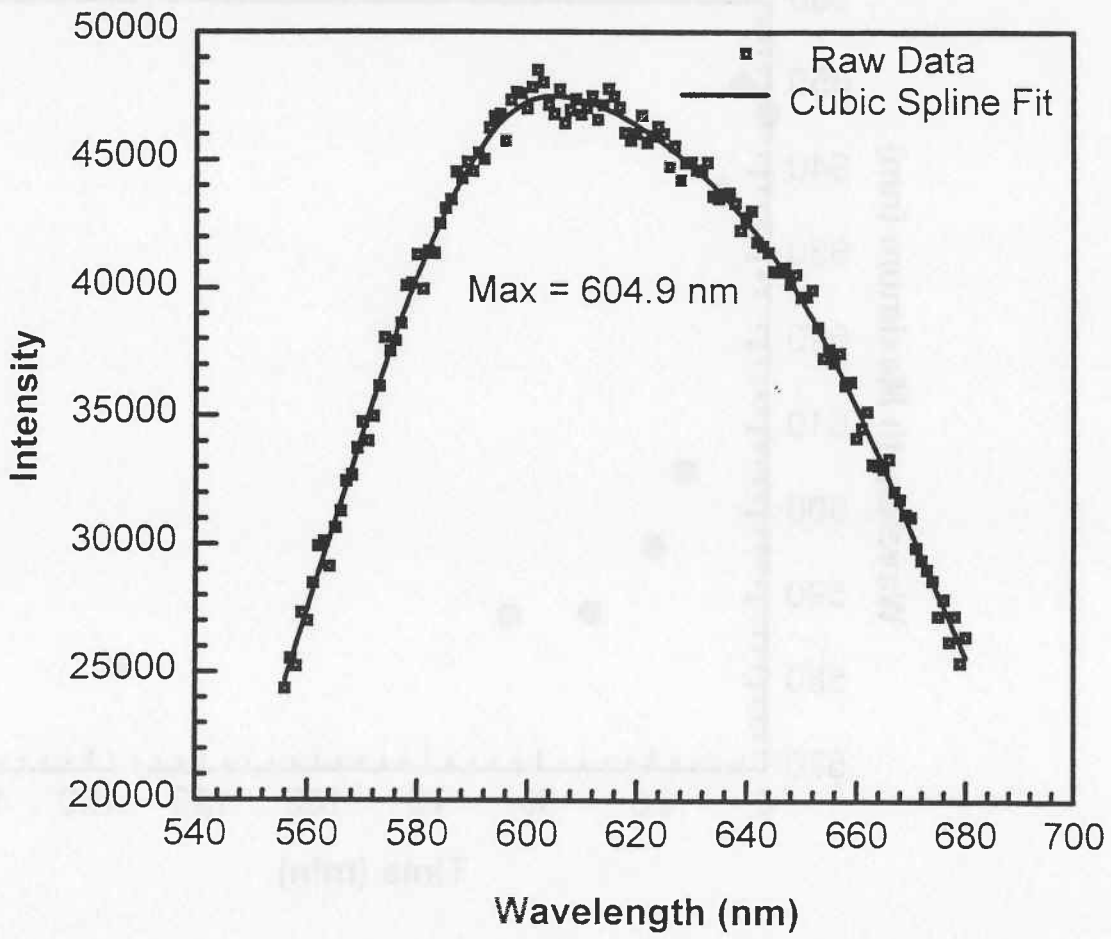
Raw Data
Cubic Spline Fit
Max = 604.9 nm
Intensity
Wavelength (nm)
50000
45000
40000
35000
30000
25000
20000
540
560
580
600
620
640
660
680
700

Figure 9.

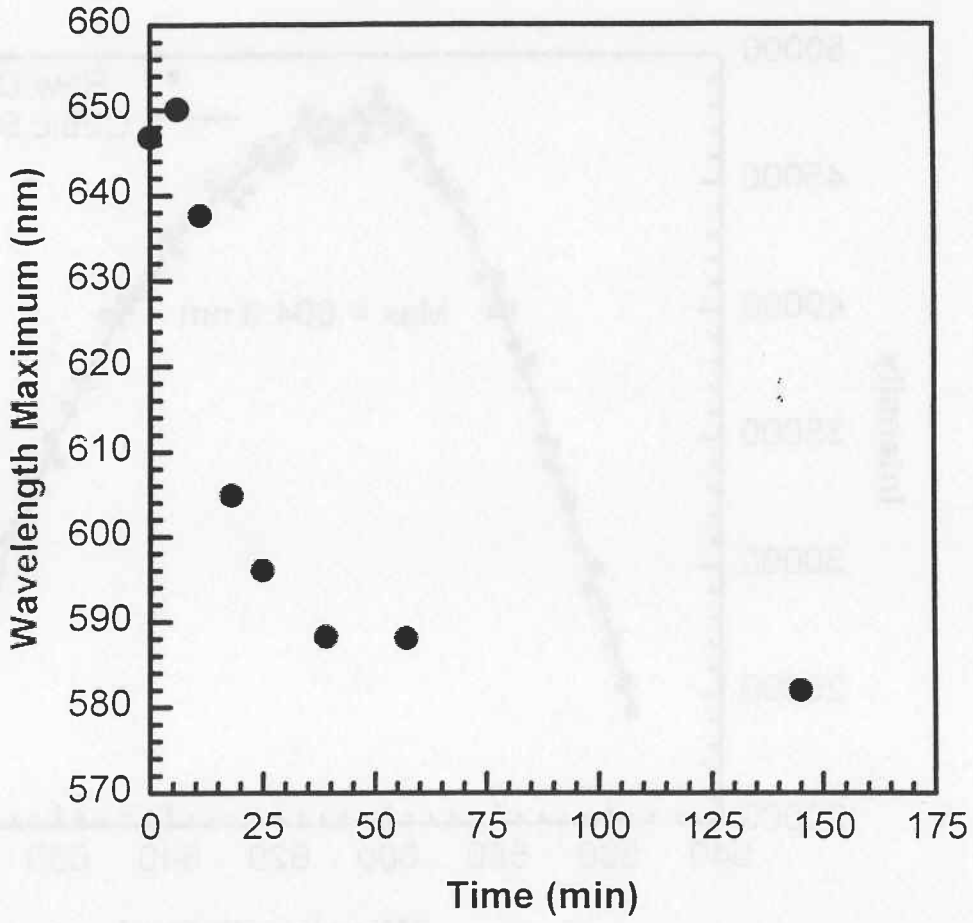
660
650
640
630
620
610
600
590
580
570
Wavelength Maximum (nm)
0
25
50
75
100
125
150
175
Time (min)

Figure 10.

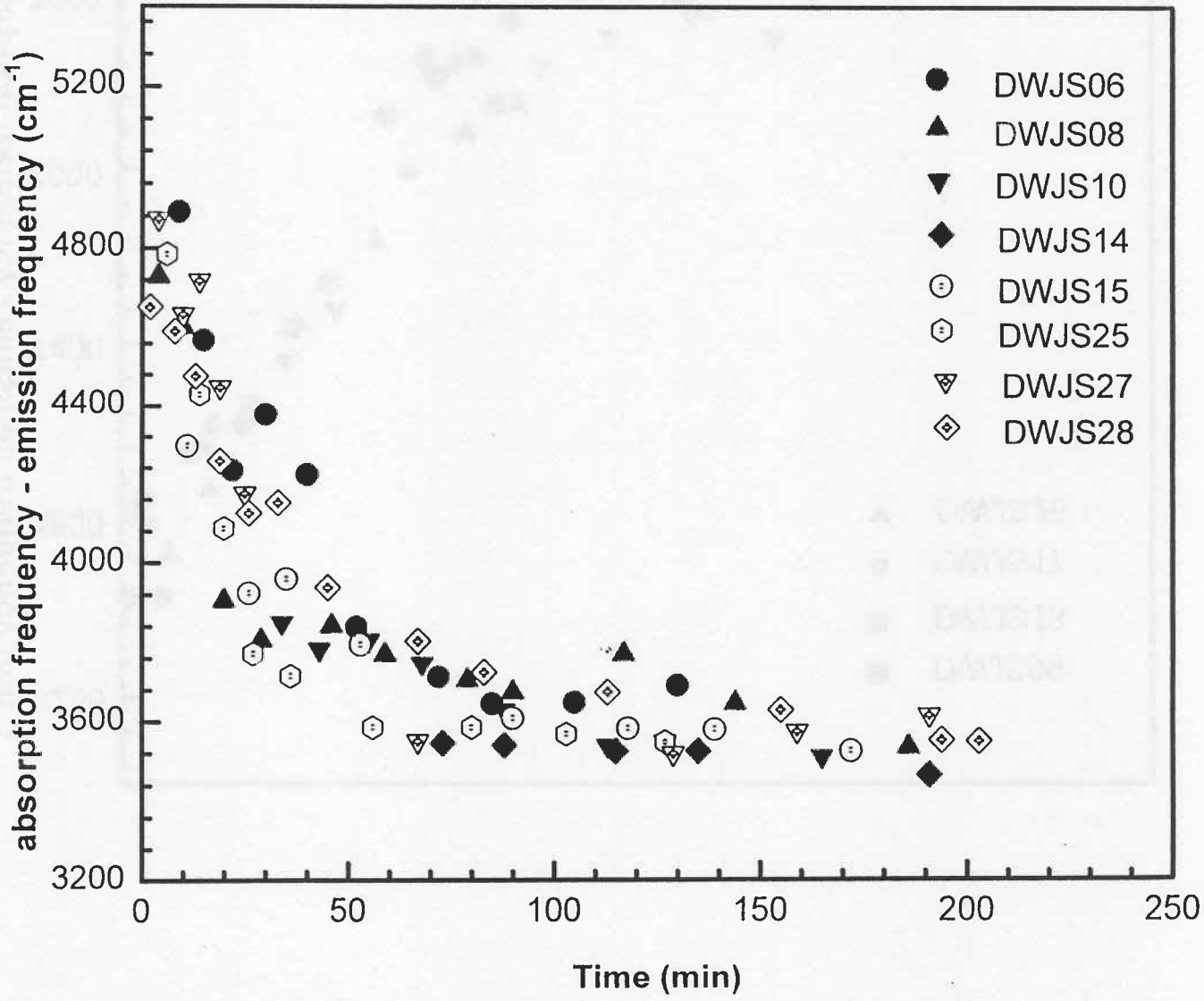
absorption frequency - emission frequency (cm^{-1})
5200
4800
4400
4000
3600
3200
0
50
100
150
200
250
Time (min)
DWJS06
DWJS08
DWJS10
DWJS14
DWJS15
DWJS25
DWJS27
DWJS28

Figure 11a

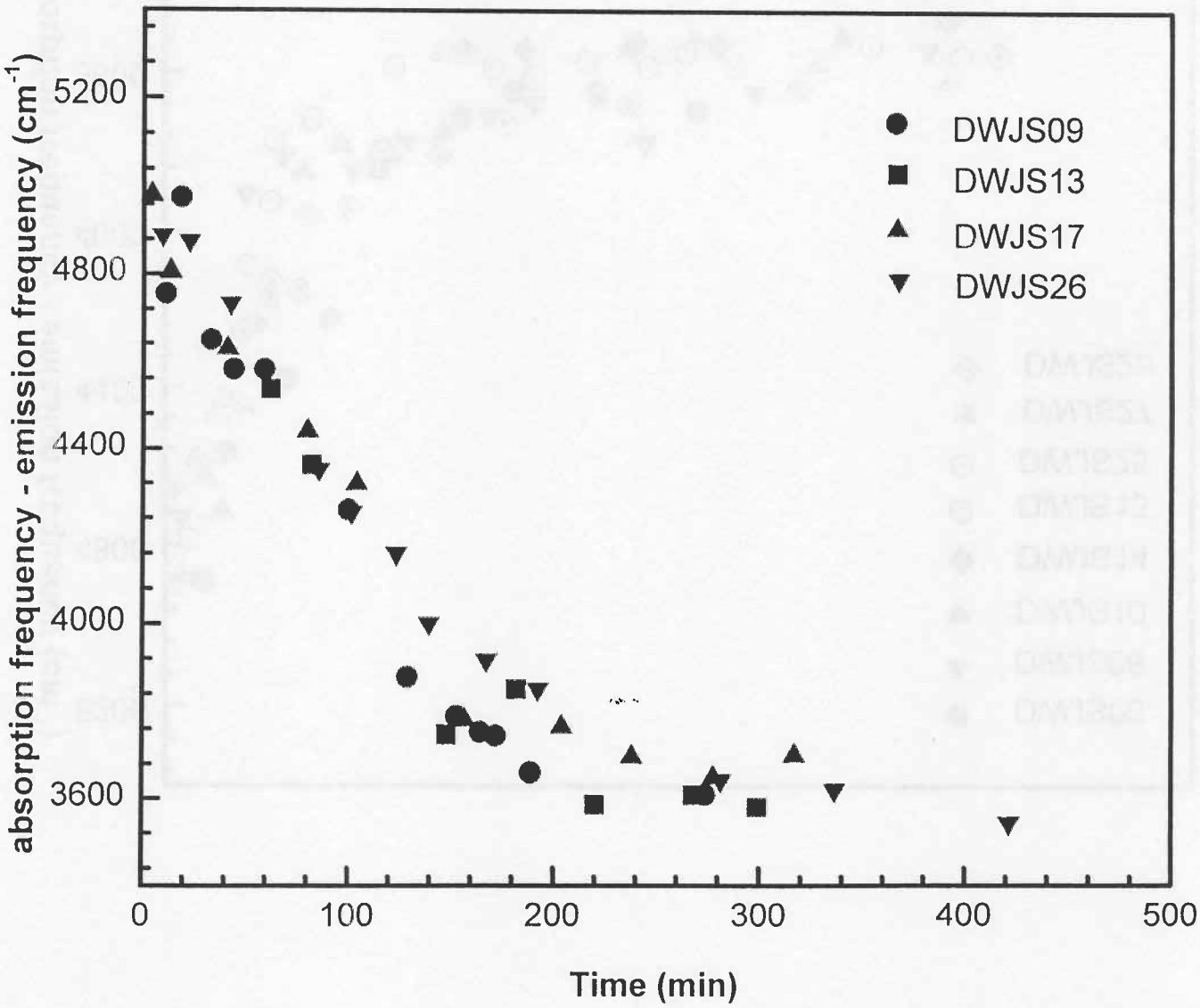
absorption frequency - emission frequency (cm^{-1})
5200
4800
4400
4000
3600
0
100
200
300
400
500
Time (min)
DWJS09
DWJS13
DWJS17
DWJS26

Figure 11b.

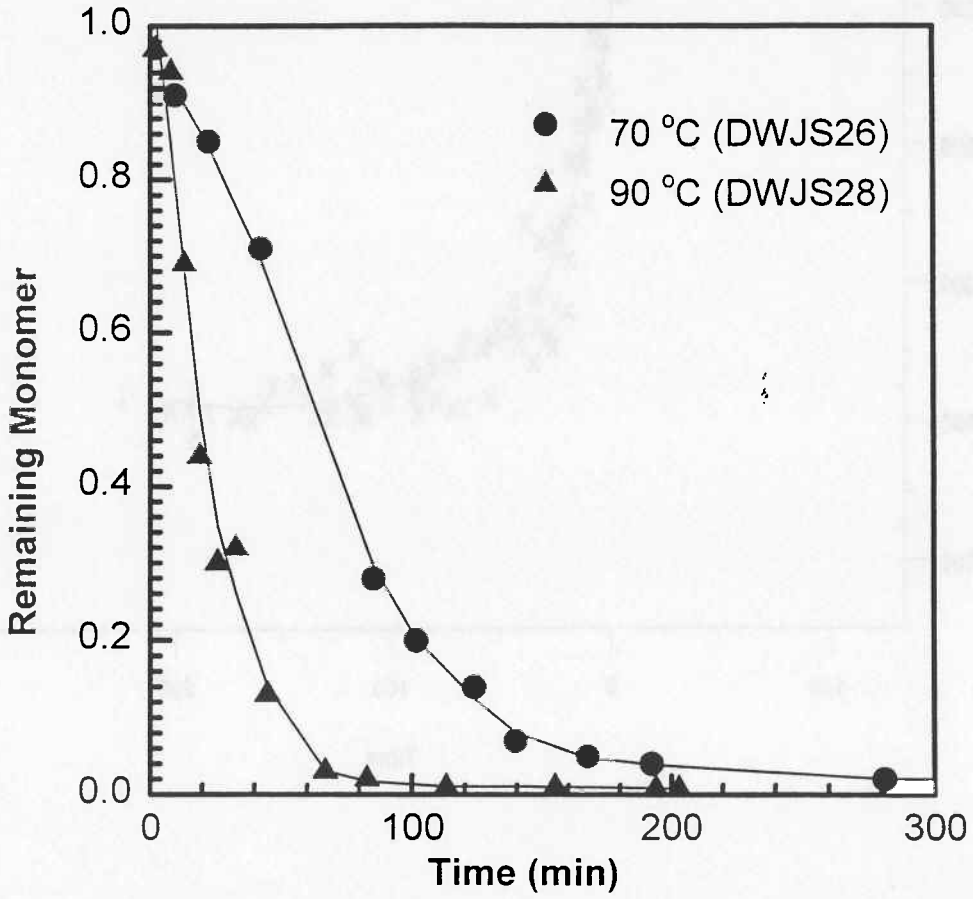
1.0
0.8
0.6
0.4
0.2
0.0
Remaining Monomer
0
100
200
300
Time (min)
70 °C (DWJS26)
90 °C (DWJS28)

Figure 12.

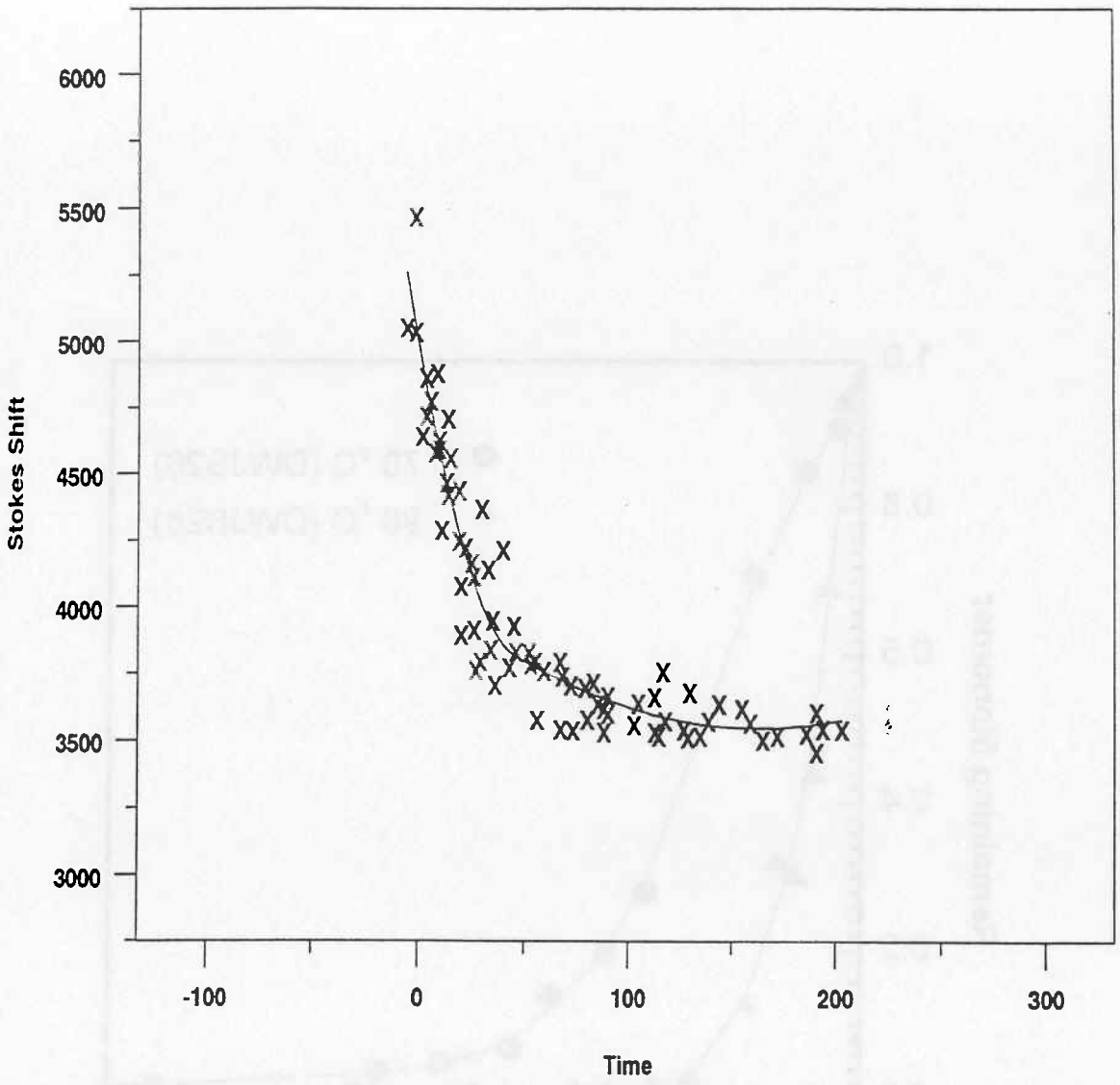
6000
5500
5000
4500
4000
3500
3000
Stokes Shift
-100
0
100
200
300
Time

Figure 13a.

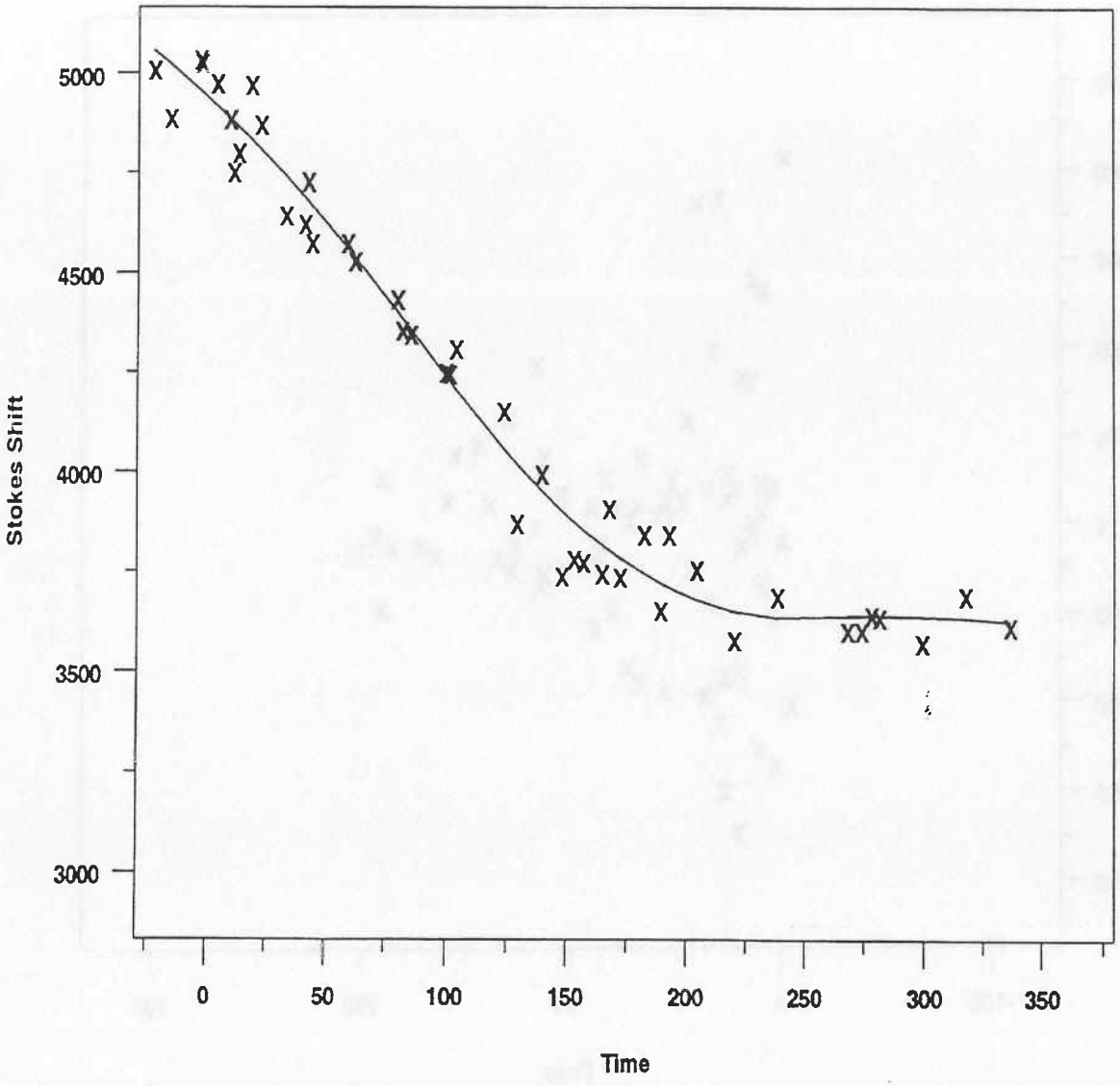
Stokes Shift
5000
4500
4000
3500
3000
0
50
100
150
200
250
300
350
Time

Figure 13b.

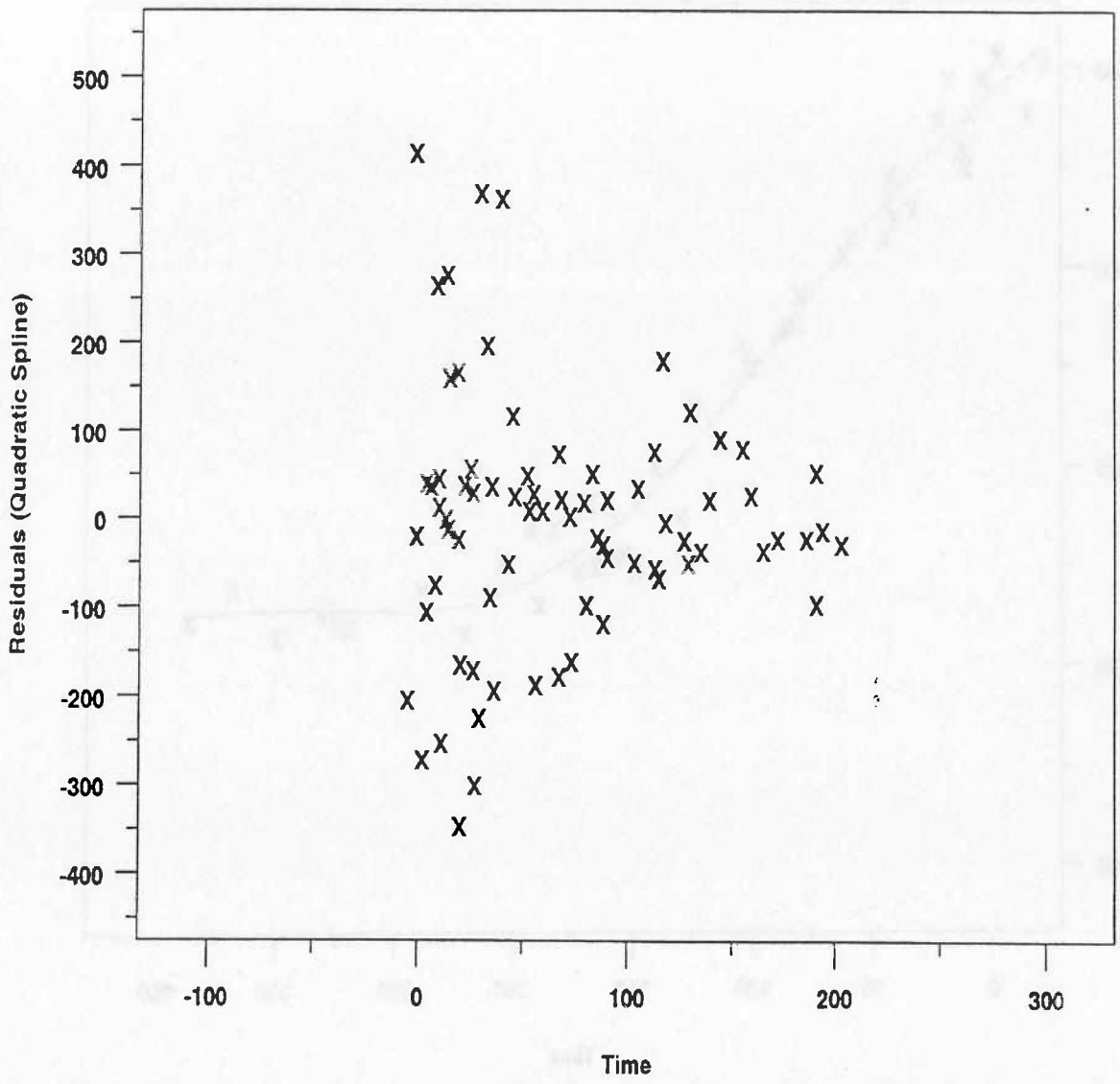
Residuals (Quadratic Spline)
500
400
300
200
100
0
-100
-200
-300
-400
-100
0
100
200
300
Time

Figure 14a.

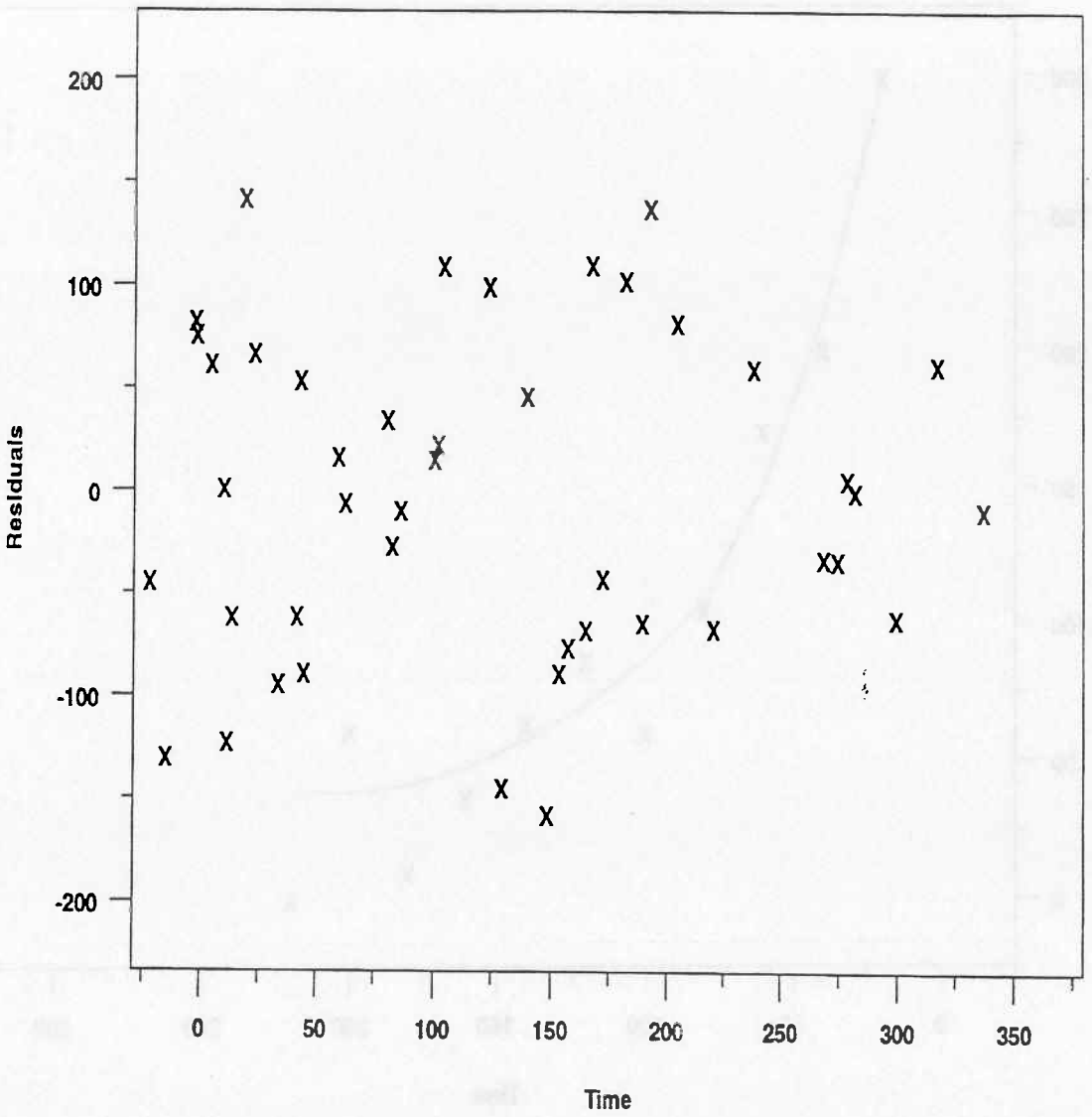

Figure 14b.

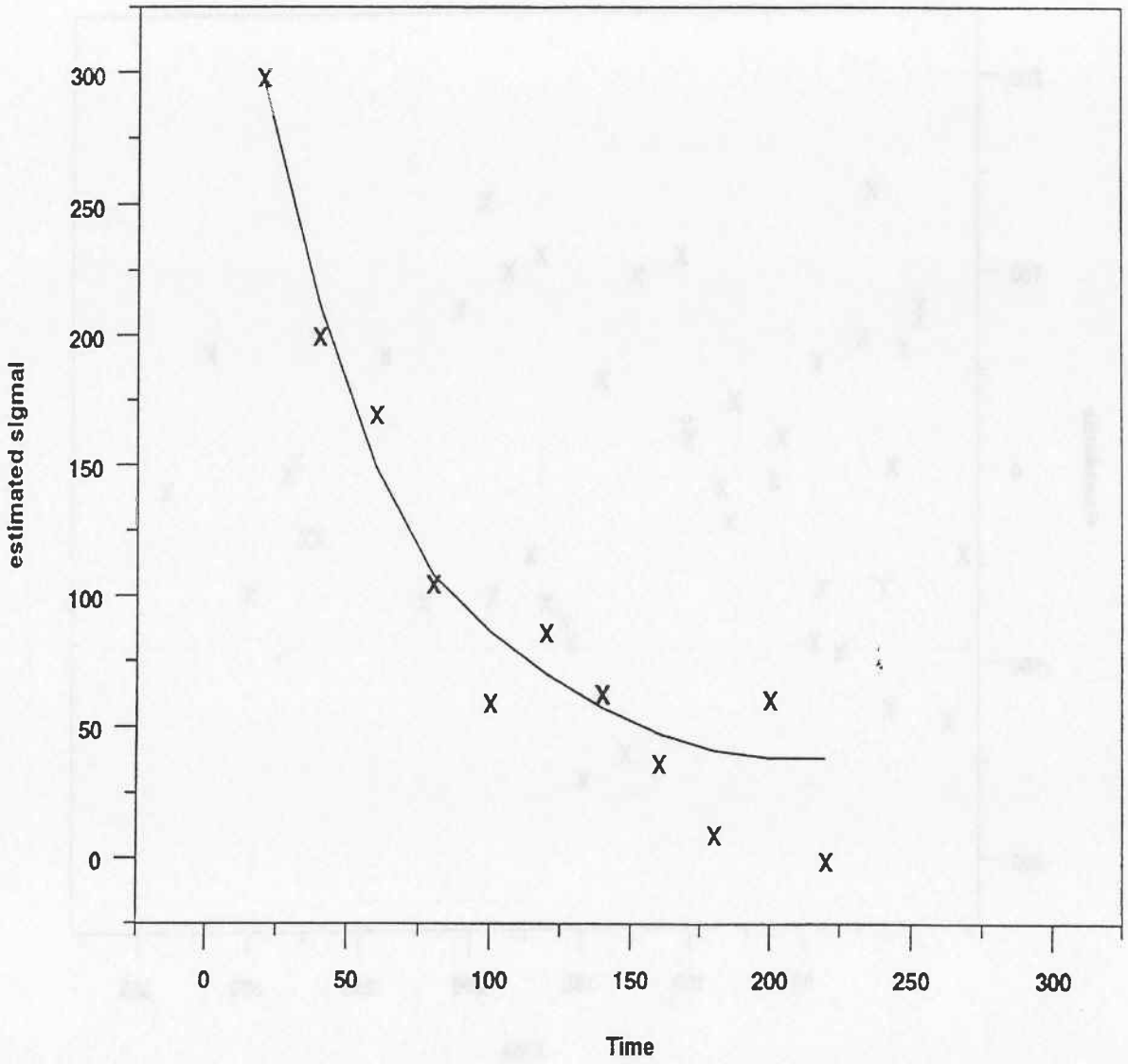
estimated sigmal
300
250
200
150
100
50
0
0
50
100
150
200
250
300
Time

Figure 15a.

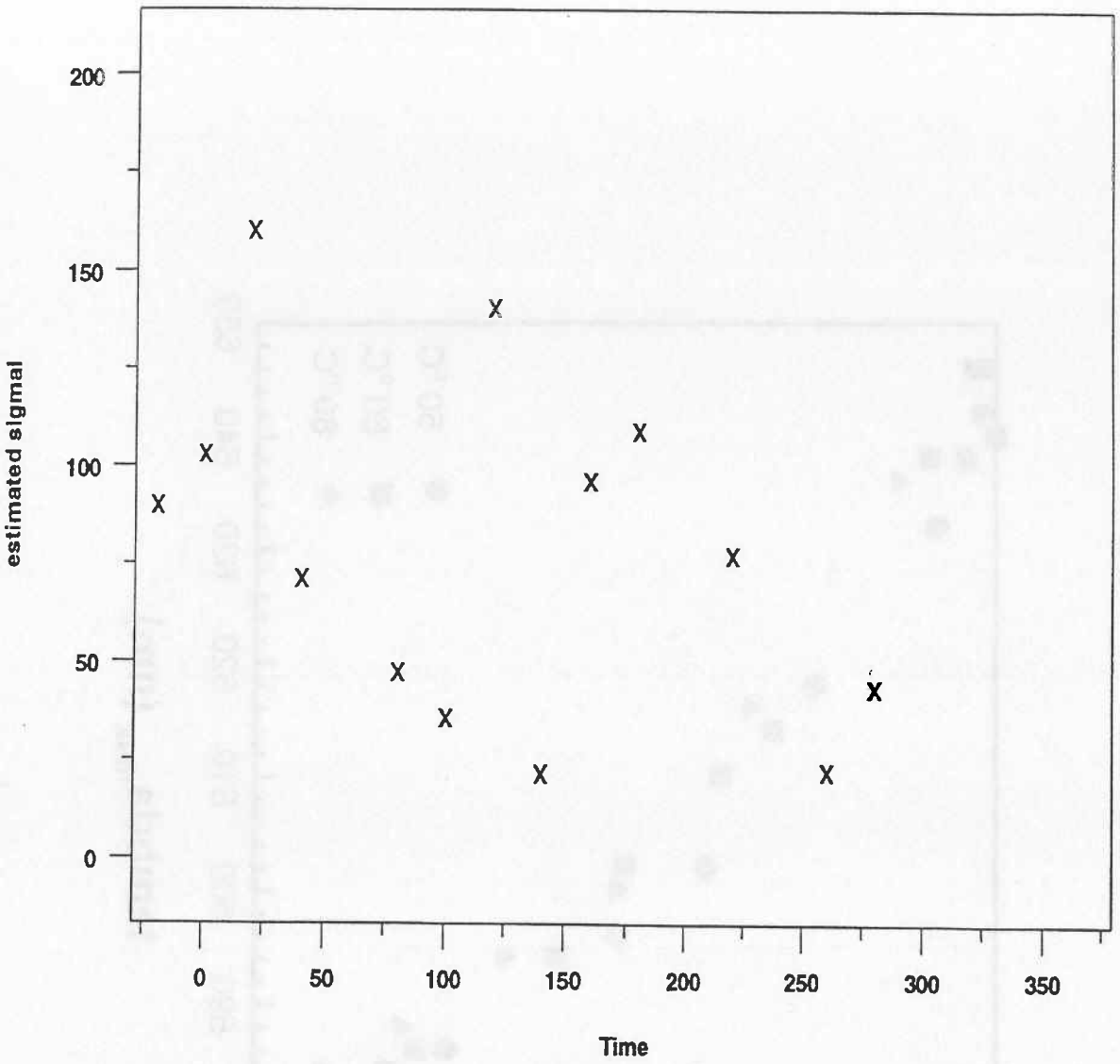
estimated sigmal
200
150
100
50
0
0
50
100
150
200
250
300
350
Time

Figure 15b.

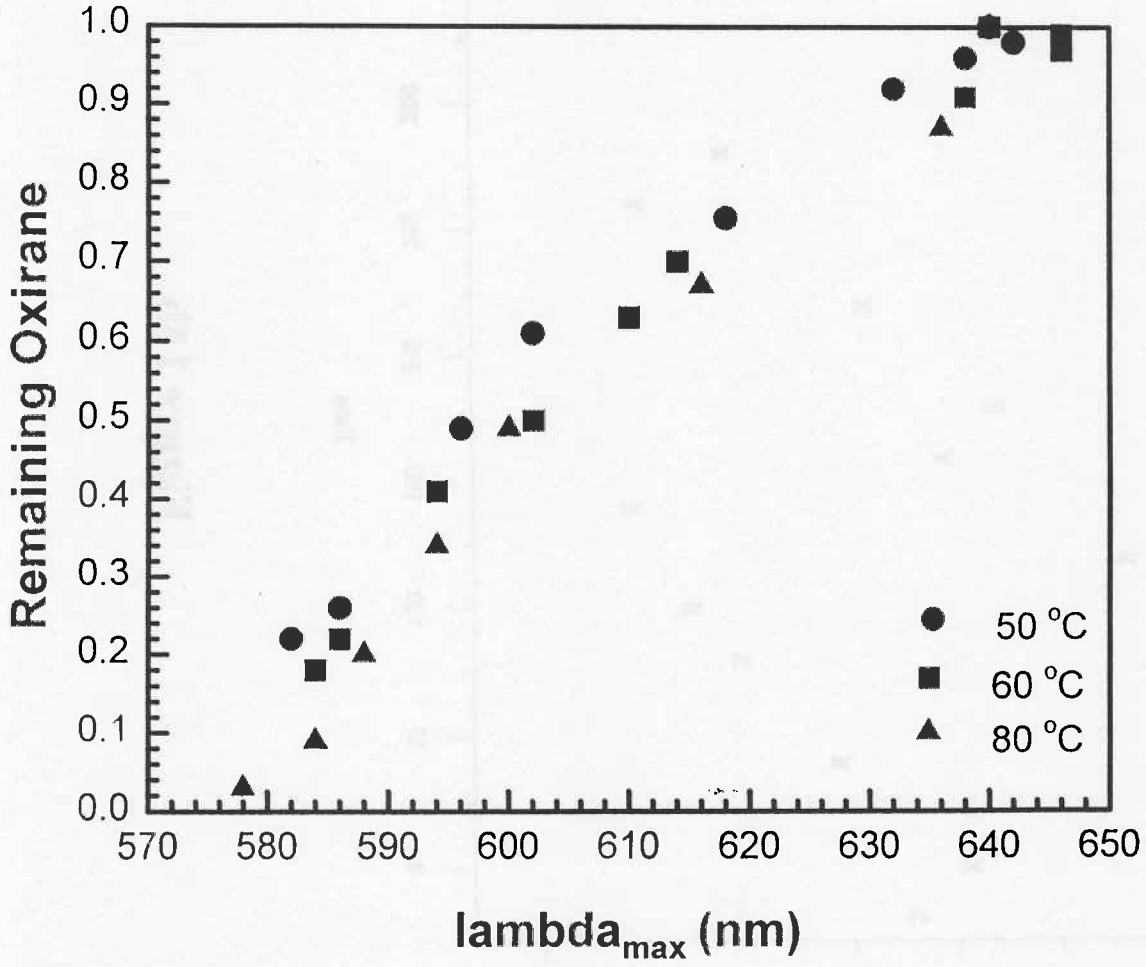
Remaining Oxirane
1.0
0.9
0.8
0.7
0.6
0.5
0.4
0.3
0.2
0.1
0.0
570
580
590
600
610
620
630
640
650
lambda$_{max}$ (nm)
50 °C
60 °C
80 °C

Figure 16.

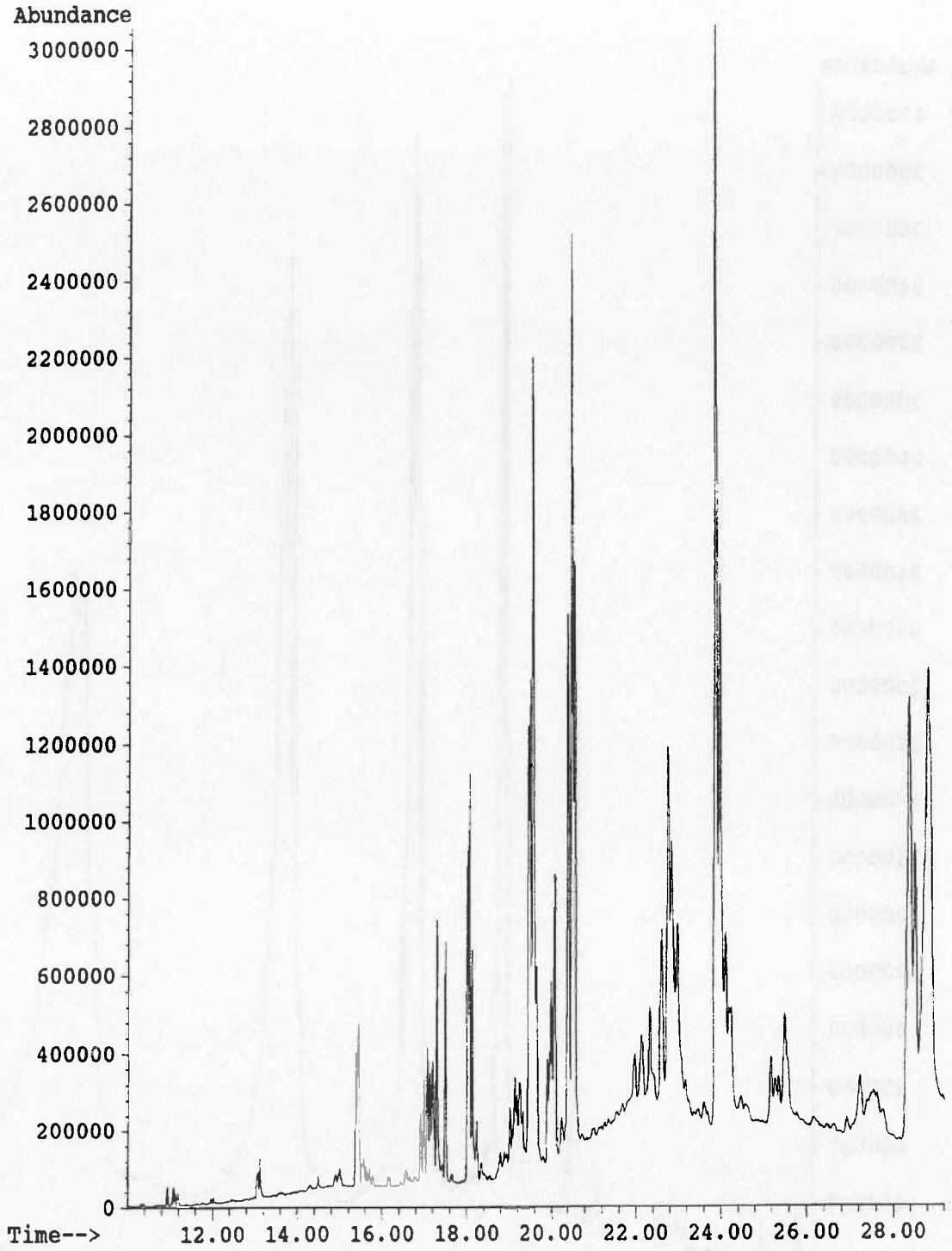
Abundance
3000000
2800000
2600000
2400000
2200000
2000000
1800000
1600000
1400000
1200000
1000000
800000
600000
400000
200000
0
Time-->
12.00
14.00
16.00
18.00
20.00
22.00
24.00
26.00
28.00

Figure 17a.

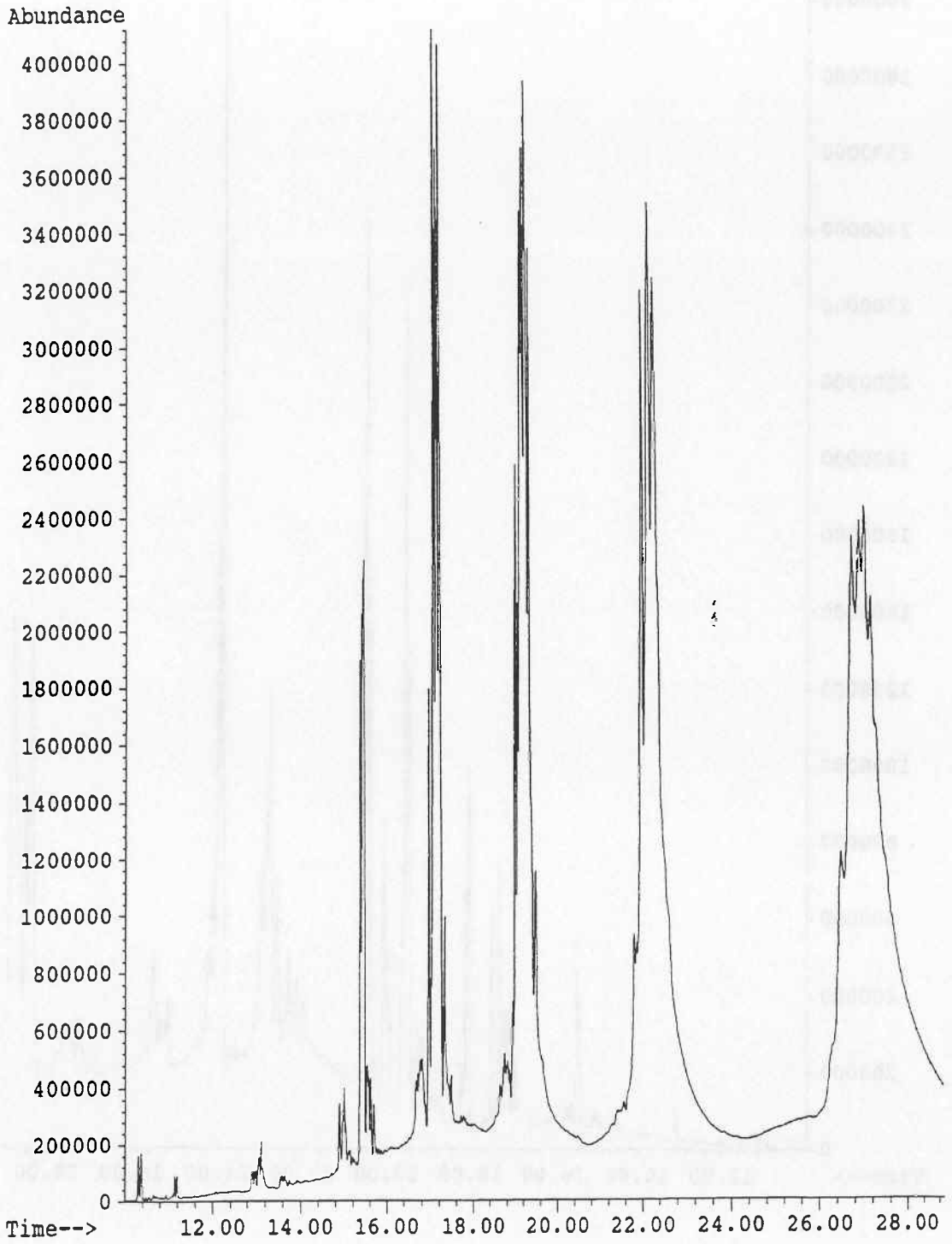
Abundance
4000000
3800000
3600000
3400000
3200000
3000000
2800000
2600000
2400000
2200000
2000000
1800000
1600000
1400000
1200000
1000000
800000
600000
400000
200000
0
Time-->
12.00
14.00
16.00
18.00
20.00
22.00
24.00
26.00
28.00

Figure 17b.

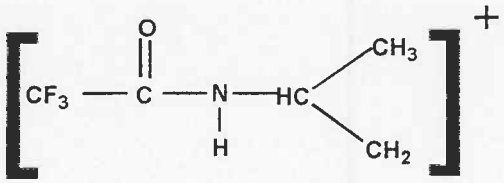

Figure 17c.

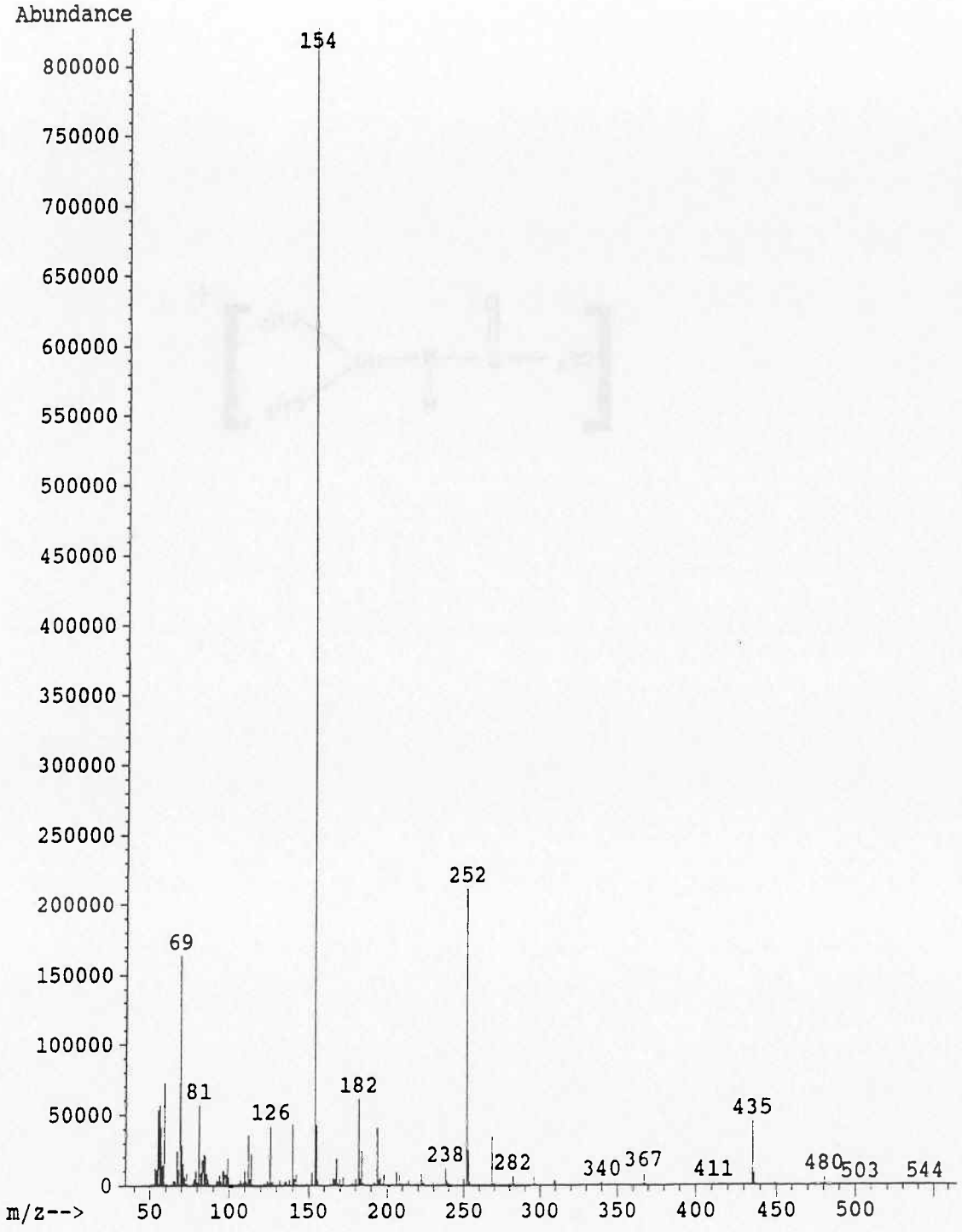
Abundance
800000
750000
700000
650000
600000
550000
500000
450000
400000
350000
300000
250000
200000
150000
100000
50000
0
m/z-->
50
100
150
200
250
300
350
400
450
500
154
252
69
81
126
182
238
282
340
367
411
435
480
503
544

Figure 18a.

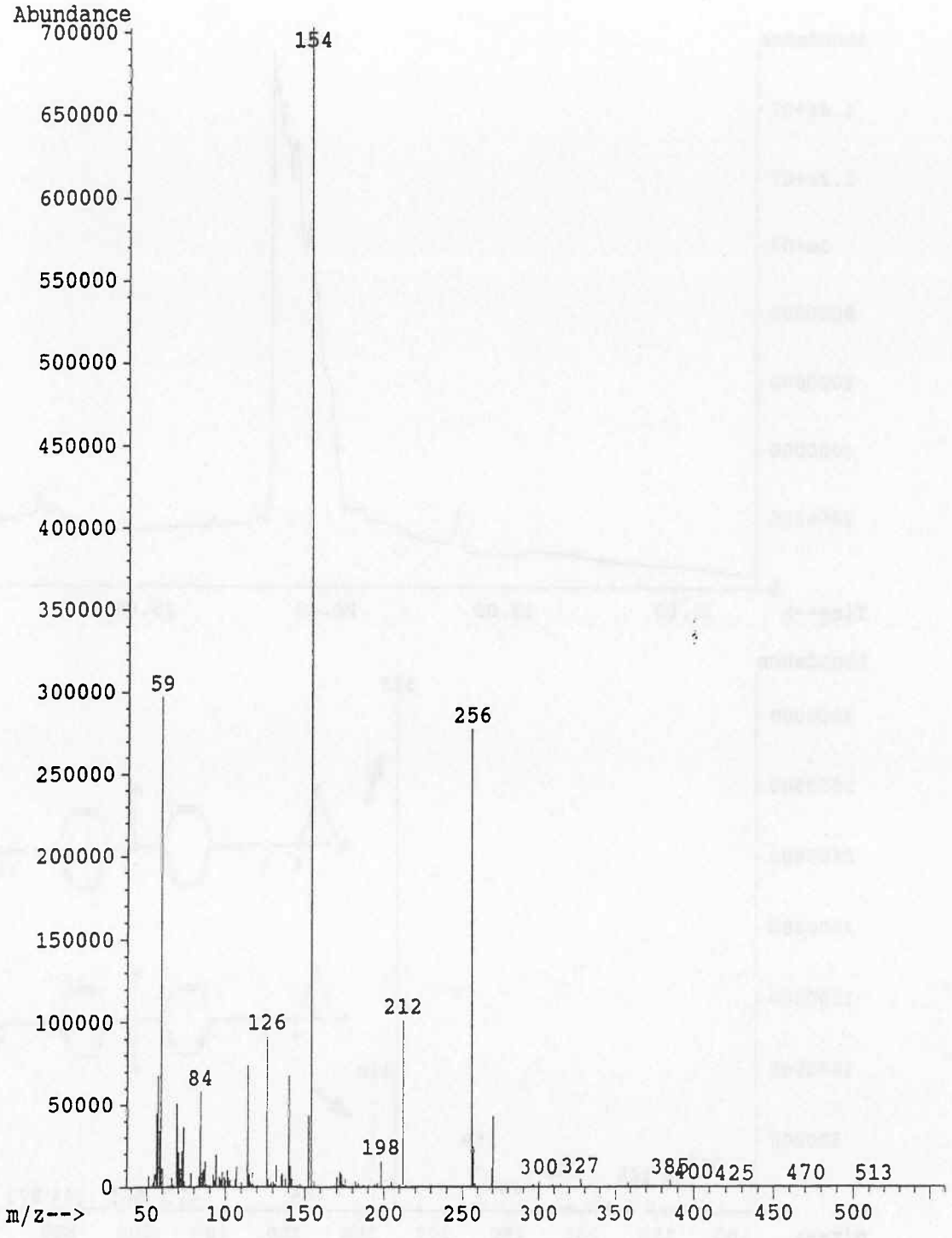
Abundance
700000
650000
600000
550000
500000
450000
400000
350000
300000
250000
200000
150000
100000
50000
0
m/z-->
50
100
150
200
250
300
350
400
450
500
154
59
256
212
126
84
198
300327
385
400425
470
513

Figure 18b.

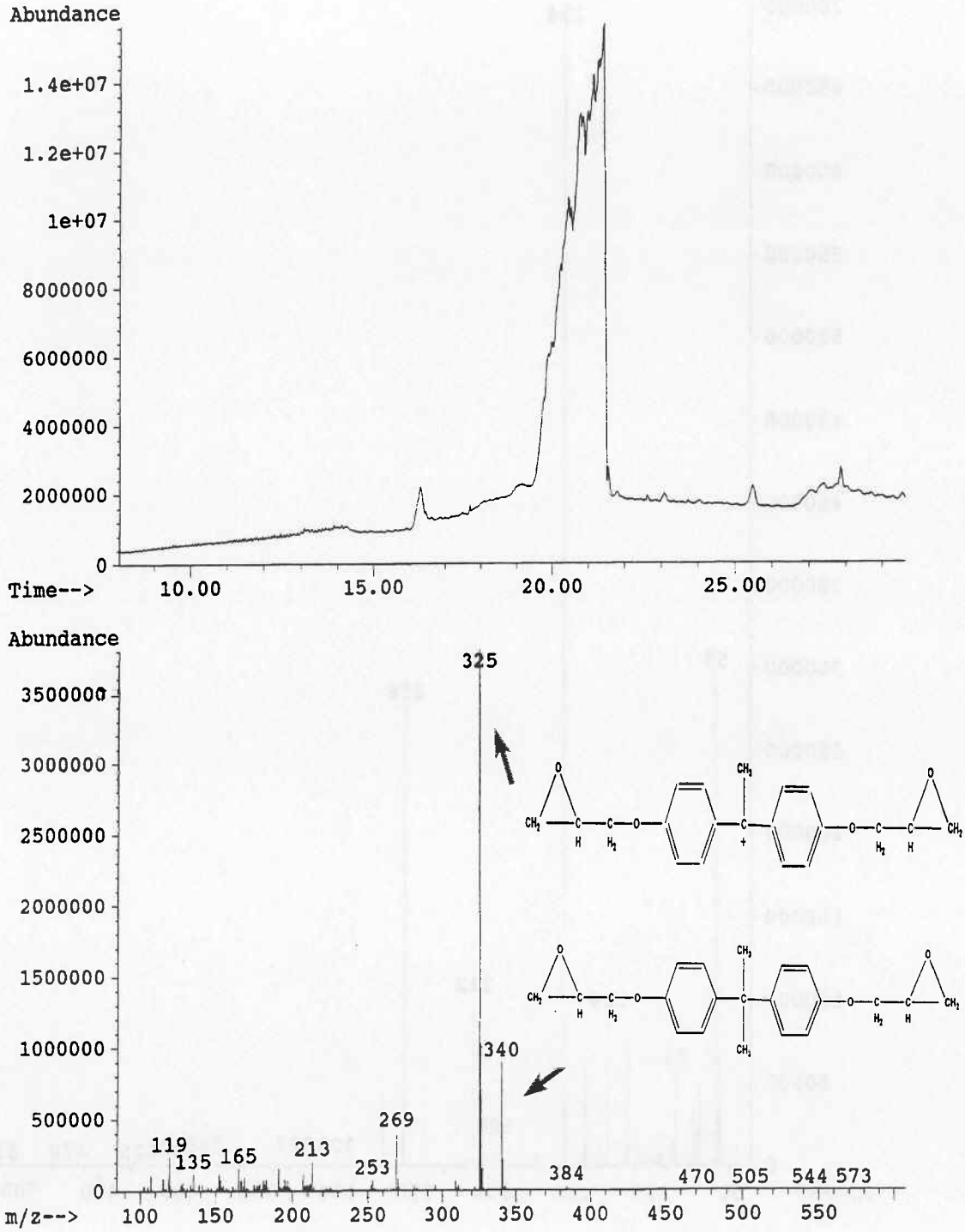

Figures 19a. & 19b.

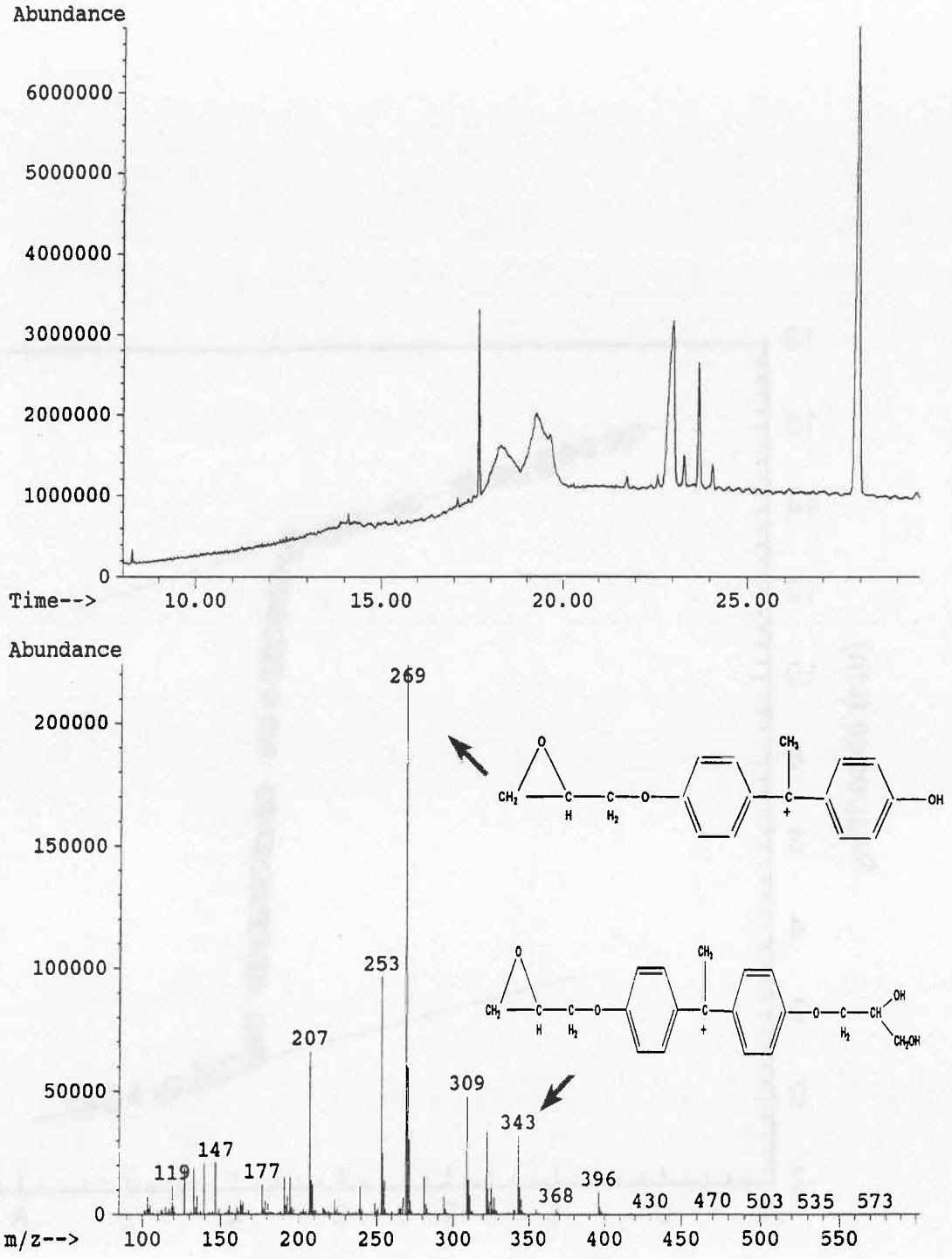

Figures 19c. & 19d.

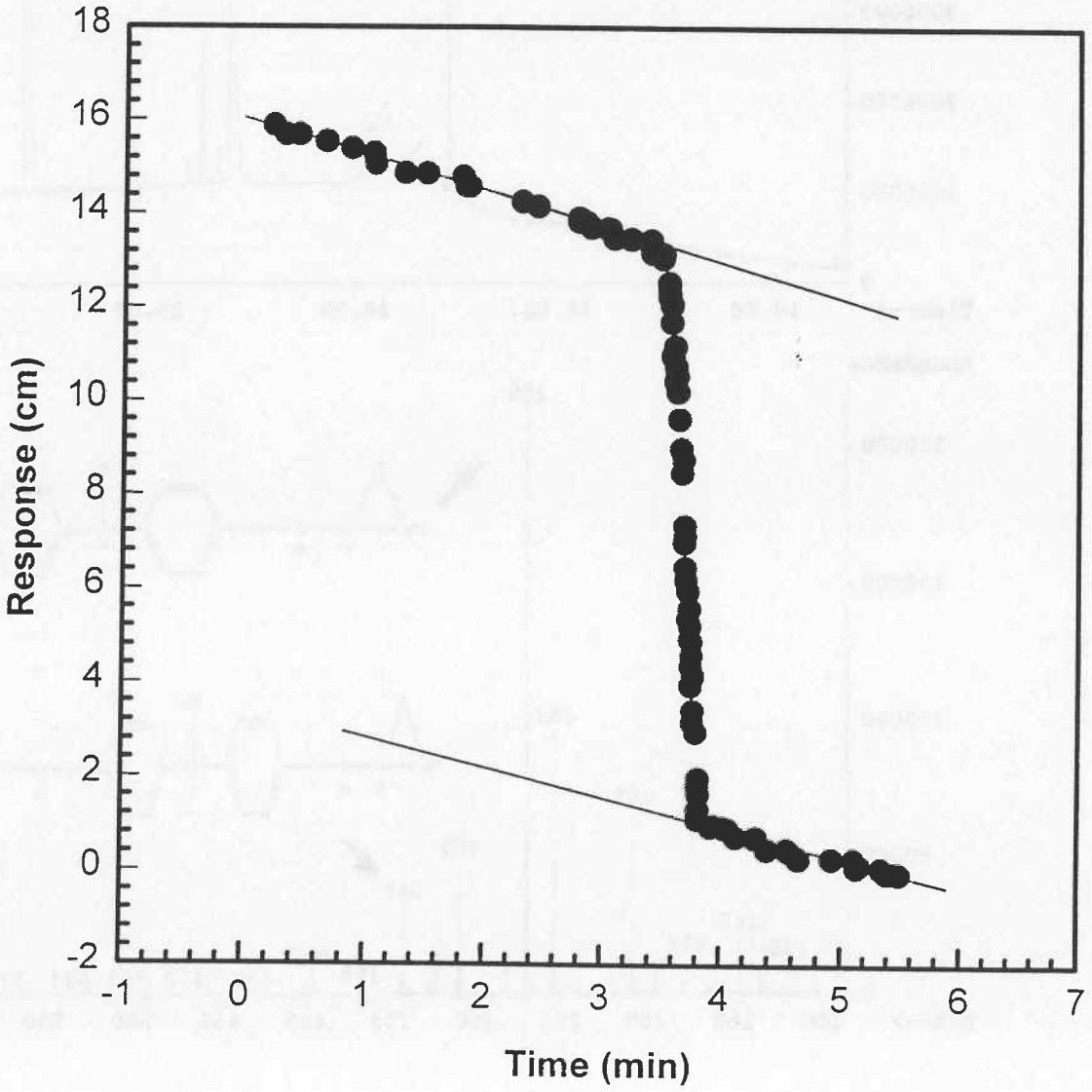

Figure 20.

Expt. Name	Cure Temp. (°C)	Outlet Pressure (psi)	Driving pressure (psi)	Number of layers
DWJS09	70	-3	14	24
DWJS13	70	-9	14	22
DWJS17	70	-3	14	24
DWJS26	70	-9	14	22
DWJS06	90	-9	18	24
DWJS08	90	-6	20	23
DWJS10	90	-6	20	23
DWJS14	90	-6	34	23
DWJS15	90	-6	6	23
DWJS25	90	-6	20	23
DWJS27	90	0	20	23
DWJS28	90	-6	20	21
DWJS24	110	-3	14	22
DWJS29	110	-3	27	24
DWJS04	120	-6	12	23
DWJS07	120	-12	20	23

Table 1.

Expt. Name	Mold Filling Time (sec)	Estimated Fiber Wetout Time (sec)	Time Resin Flow Stopped (sec)
DWJS09	1120	498	1120*
DWJS13	75	19	605*
DWJS17	960	427	1125
DWJS26	1390	618	3090
DWJS06	75	19	605*
DWJS08	165	41	305*
DWJS10	270	68	305*
DWJS14	95	42	190*
DWJS15	short shot, but reached sensor	600 (based on pt. at 640 nm)	0
DWJS25	430	108	915
DWJS27	230	58	360
DWJS28	55	14	70
DWJS24	140	35	470
DWJS29	205	91	745
DWJS04	110	28	305*
DWJS07	235	104	605*

* Estimated.

Table 2.

Sample	WSO response: (mm) of chart dist. ± 2σ	Ratio of Sample & WSO responses	Sample weight (mg)	x 10^3 mg H_2O per mg of sample
Old Amine	126 ± 18	0.595	32	7.65
Old Amine	126 ± 18	1.016	61	6.86
New Am.	126 ± 18	0.317	82	1.59
New Am.	126 ± 18	0.365	88	1.71
Old Epoxy	72 ± 10	0.208	19.9	4.30
Old Epoxy	72 ± 10	0.431	29.6	5.99
New Epox.	72 ± 10	0.139	65.3	0.876
New Epox.	72 ± 10	0.167	117.5	0.585

Table 3.